Oblique rifting triggered by slab tearing and back-arc extension : the case of the Alboran rift in the eastern Betics

Marine Larrey[1,2], Frédéric Mouthereau[1*], Damien Do Couto[3], Emmanuel Masini[4], Anthony Jourdon[5], Sylvain Calassou[2] and Véronique Miegebielle[2]

[1]Université Paul Sabatier, Géosciences Environnement Toulouse, GET UMR 5563, Toulouse, France.

[2]TOTAL S.A., Centre Scientifique & Technique Jean Féger, Pau, France.

[3]Sorbonne Université, CNRS-INSU, Institut des Sciences de la Terre Paris, ISTeP UMR 7193, F-75005 Paris, France.

[4]M&U sas, France.

[5]Institute of Geophysics, Ludwig-Maximilians-Universität München, Munich, Germany.

Corresponding author: Frédéric Mouthereau (frederic.mouthereau@get.omp.eu)

Abstract

The tectonic evolution of highly oblique continental margins that result from back-arc extension above lithospheric STEP faults is poorly understood. Here, we investigate the case of the Alboran margin in the eastern Betics characterized by crustal thinning of 15-10 km, oblique to the direction of slab retreat. The current deformation patterns indicate that oblique back-arc rifting is underway. However, it is unclear whether these conditions are those that prevailed during the formation of the metamorphic domes and intramontane basins. We review the temporal and spatial evolution of Neogene sedimentary basins and brittle deformation in the eastern Betics, and exploit offshore seismic reflection lines to propose a crustal-scale section across the oblique margin. The history of sediment infill and rates of subsidence combined with the analyses of fault slip data, confirm that brittle extension oriented from N20°E to EW occurred during an interval spanning from the Serravallian-early Tortonian to the late Tortonian (14-8 Ma). This extension is found associated with both normal and strike-slip regimes and the evolution of the strike-slip corridors flanking the metamorphic domes. The transtensional model forms a coherent scheme linking the ductile deformation associated with metamorphic domes and the formation of EW- and NW-SE/NNW-SSE-directed sedimentary basins in the brittle upper crust during the Tortonian. The oblique extension, which is closely associated with STEP faulting, occurred during the regional convergence between Africa and Iberia since the Miocene. Only recently, around 8 Ma, the slab detached, leading to local tectonic inversion. Such a type of narrow oblique rifted margin associated with transform-like plate boundaries is not unique but is expected to be hardly preserved in the geological record due to the transient nature of retreating subduction systems.

1 Tear faulting and the formation of oblique transform margin in the Betics

33 Lithospheric tear faults or subduction-transform edge propagator (STEP) faults are propagating strike-slip faults that

34 accommodate the differential motion between the retreating subduction zone and the overriding back-arc plate (Govers

35 and Wortel, 2005). Because of the relative motion between back-arc and surrounding plates, they are also propagating

36 strike-slip faults defined by a sharp contrast in crustal thickness. As noted by Govers and Wortel (2005) such oblique

37 fault boundaries do not necessarily form proper transform plate boundaries but broad zones of distributed deformation,

38 accommodating differential trench-parallel extension, strike-slip motion and rotation. In case the lithospheric tear

39 propagates within the continent-ocean transition, a narrow continental margin forms highly oblique to the direction of

40 back-arc extension. This is documented, for instance, in the Carribean, along the transcurrent Carribean-South

41 America plate boundary (Pindell and Kennan, 2009) or on the margin of the South Orckney microcontinent, along the

42 Scotia-Antarctic plate boundary (Dalziel et al., 2013). Despite the large-scale kinematic picture is relatively well

43 understood, there are only few places where continental crustal deformation associated with this peculiar type of slab-

44 edge continental rift system can be studied.

45 Here, we focus on the Betic Cordillera, on the northern boundary of the Gibraltar arc (**Figs 1 and 2**). There, a rifted

46 margin, defined by decreasing crustal thickness from 35 to 10 km in the Alboran basin (Diaz et al., 2016), is seen to

47 develop above a STEP fault (Badji et al., 2014; Gallais et al., 2013; Jolivet et al., 2021a; Mancilla et al., 2015a). The

48 tectonic expression of the transcurrent deformation during crustal extension above the lithospheric tear is however

49 controversial. On the one hand, low-angle ductile extensional detachments with a top-to-the-west sense of shear are

50 the main features accommodating deformation in the overriding plate. Yet, a-type metamorphic domes in the lower

51 crust, elongated parallel to the E-W direction (**Fig. 1**), are viewed to express the transtensional deformation at the tip

52 of propagating tear (Pourhiet et al., 2012). On the other hand, strike-slip faulting is interpreted as a late brittle

53 deformation feature associated with E-W crustal strike-slip brittle faults between the metamorphic domes in the eastern

54 Betics (Alpujarras corridor ; Sanz de Galdeano and Vera, 1992; Sanz de Galdeano et al., 1985; Martínez-Martínez et

55 al., 2006) and in the western Betics (e.g. Torcal corridor ca et al., 2016) unrelated to ductile deformation (**Fig.

56 1**). In line with the latter interpretation, the dextral motion these strike-slip faults accommodate is assumed to be

57 modest, reflecting a recent post-8 Ma kinematic change that accompanies the end of slab retreat, and onset of

58 compression in the Gibraltar Arc (Do Couto et al., 2014; d'Acremont et al., 2020; Jolivet et al., 2021a; Martínez-

59 García et al., 2017).

60 The lack of structural, temporal constraints and quantification of belt-parallel motion along these faults indicates,

61 however, that we do not yet fully understand their link with the long-term evolution of slab tearing and margin

62 formation. For instance, the current deformation patterns brings critical evidence that both strike-slip faulting and

63 extension operate synchronously, so that brittle strike-slip faulting and ductile extension might reflect the same

64 tectonic episode. This is argued by ongoing extension illustrated by the west-directed GPS velocities increasing

65 westwards, and the west-directed displacements increasing towards the Alboran domain revealing active right-lateral

66 shear deformation (**Fig. 2**). The current transtensional deformation across the Betic Cordillera is also shown by the

67 current stress regime defined by extension direction highly oblique (max. 20°) to the Betic structural trend (or 70°

68 spanned by the direction of extension and normal of the rift trend). Right-lateral transtensional deformation in the

69   Betic agrees with evidence for west-directed lateral extrusion of the Alboran Basin (Borque et al., 2019; Palano et al.,

70   2015). In the east, the extrusion is accommodated by left-lateral strike-slip displacement along the Eastern Betic Shear

71   Zone (EBSZ; Borque et al., 2019), which is shaped by the Carboneras Fault (CF) and Palomeras Fault (PF). This fault

72   extends offshore, across the Alboran Sea, in the larger Trans-Alboran Shear Zone (De Larouzière et al., 1988; Stich

73   et al., 2006) moving at ~4 mm/yr, equivalent to the regional 5 mm/yr NW-directed convergence between Africa

74   (Nubia) and Europe (**Fig. 2**; Echeverria et al., 2013; Koulali et al., 2011; Nocquet, 2012; Palano et al., 2015, 2013;

75   Vernant et al., 2010). Here, we hypothesize that the present-day oblique extension patterns is at play since the Miocene

76   and explain the formation of the narrow Alboran rifted margin.

77
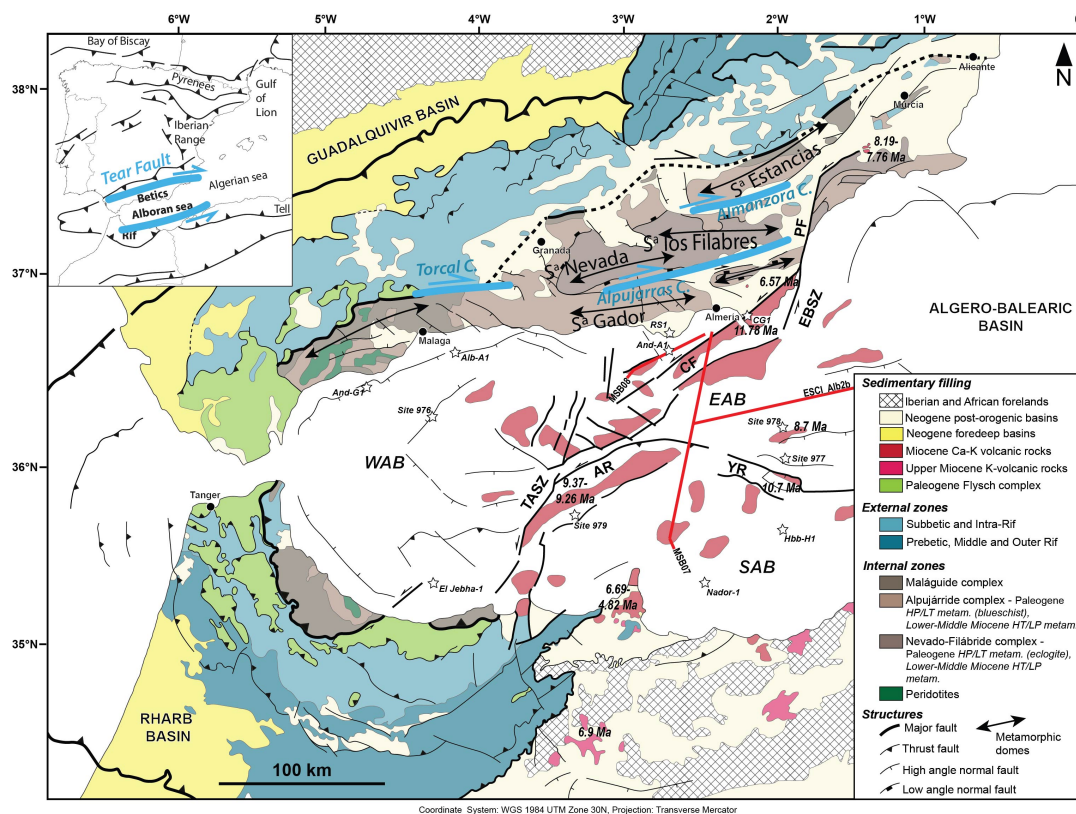
78

79   **Figure 1** : Geological map of the Betic-Rif arc. Main tectonic units and age of volcanism as well as major structures
80   and Neogene sedimentary basins are shown. The studied offshore seismic lines (red) is displayed as well as offshore
81   wells and ODP sites (★) for stratigraphic calibration in the East (EAB), South (SAB) and West Alboran basins
82   (WAB). CF: Carboneras Fault; PF : Palomeras Fault; AR: Alboran Ridge; YR: Yusuf Ridge; EBSZ : East Betic Shear
83   Zone; TASZ: Trans-Alboran Shear Zone.

84

85   Only recently high-resolution 3D numerical models have been able to predict the deep structure of oblique rift

86   domains. These models can be used as a guide to re-evaluate the evolution of the Betic region. 3D models by Jourdon

87   et al. (2021) predict that oblique extension results in narrow rifted margins, strike-slip faults and corridors coupled

88   with subsident pull-apart basins, normal faults and block rotations (**Fig. 3**). The recognition of block rotation in the

89   Betic arc (Crespo-Blanc et al., 2016; Platzman, 1992), strike-slip corridors (**Fig. 1**) and NW-SE normal faulting which

90   defines extension direction highly oblique to the margin, (Galindo-Zaldivar et al., 2003; **Figs 1 and 2**) all support this

91   view. The simulations of Jourdon et al. (2021) also show that the deeper ductile crust experiences thinning (vertical

92   flattening) and stretching perpendicular to the strike of the margin in accordance with stretching lineations parallel to

93   the metamorphic domes and low-angle detachments (**Fig. 3**). Other types of 3D numerical experiments show that

94   sediment loading of strike-slip faults can result in assymetric flexural basin with apparent normal fault throw

95   (Neuharth et al., 2021) that can be mistakenly interpreted as resulting from orthogonal extension. Asymmetric basins

96   are indeed intriguing characteristics of intramontane basins in the Betics (Meijer et al., 2013; Do Couto et al., 2014).

97   Although primarily found associated with divergent plate boundaries e.g. in the Gulf of California (Fossen et al., 2013;

98   Fossen and Tikoff, 1998) highly oblique extension is also documented in active transform regions along the San

99   Andreas Fault (Teyssier and Tikoff, 1998) or the North Anatolian Fault in Marmara Sea (Okay et al., 2004). A detailed

100   analysis of highly oblique rifting deformation in the Gulf of California recognises similar tectonic elements as for the

101   Betics, such as extensional detachment systems orthogonal to the divergence and upper crustal folds trending parallel

102   to the divergence (Fossen et al., 2013).

103

104
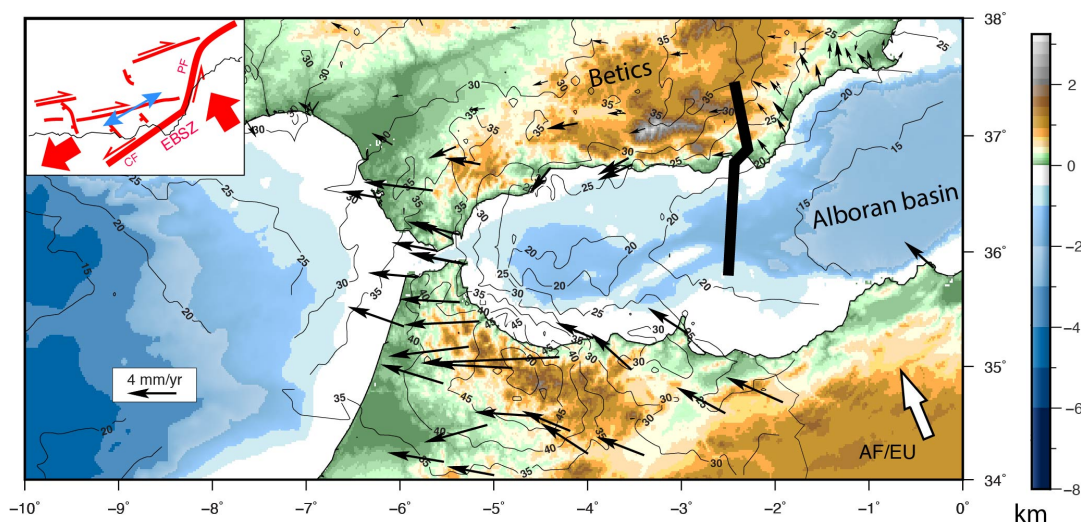
105   **Figure 2** : Present-day kinematics in the Betic-Rif arc and eastern Betic Cordillera (inset). GNSS-based displacements

106   in the Abloran block and northern Africa shown in a fixed Eurasian reference frame (black arrows after Palano et al.,

107   2015) are oblique to the AF/EU plate convergence (white arrow) inferred from plate tectonic Morvel model (Argus et

108   al., 2011). Labelled contours depict the crustal depth given in kilometers as inferred from deep seismic profiles and

109   receiver functions analysis (Diaz et al., 2016). In the eastern Betic (inset), W-directed stretching is taken up by EW-

110   directed right-lateral strike-slip fault and NW-SE normal faults. Extension direction resolved from focal mechanisms

111   (blue arrows) are after (Stich et al., 2006). CF: Carboneras Fault; PF : Palomeras Fault; AR: Alboran Ridge; YR:

112   Yusuf Ridge; EBSZ : East Betic Shear Zone; TASZ: Trans-Alboran Shear Zone.

113

114   Several tectonic features need further discussion however. First, the relevance of strike-slip faulting in the past is

115   debatable as only a few occurrence of crustal-scale strike-slip faults are mapped. Second, the detail of the temporal

116   and spatial relationships between the formation of the oblique/transform margin and STEP faulting remain elusive.
117   We here review the temporal and spatial evolution of Neogene intramontane sedimentary basins and related brittle
118   deformation in the eastern Betics. In addition, we exploit offshore seismic reflection lines to propose a new crustal-
119   scale section across the oblique margin. Based on these constraints we present a tectonic scenario for the formation of
120   the high-obliquity rift margin in back-arc setting controlled by STEP faulting.
121
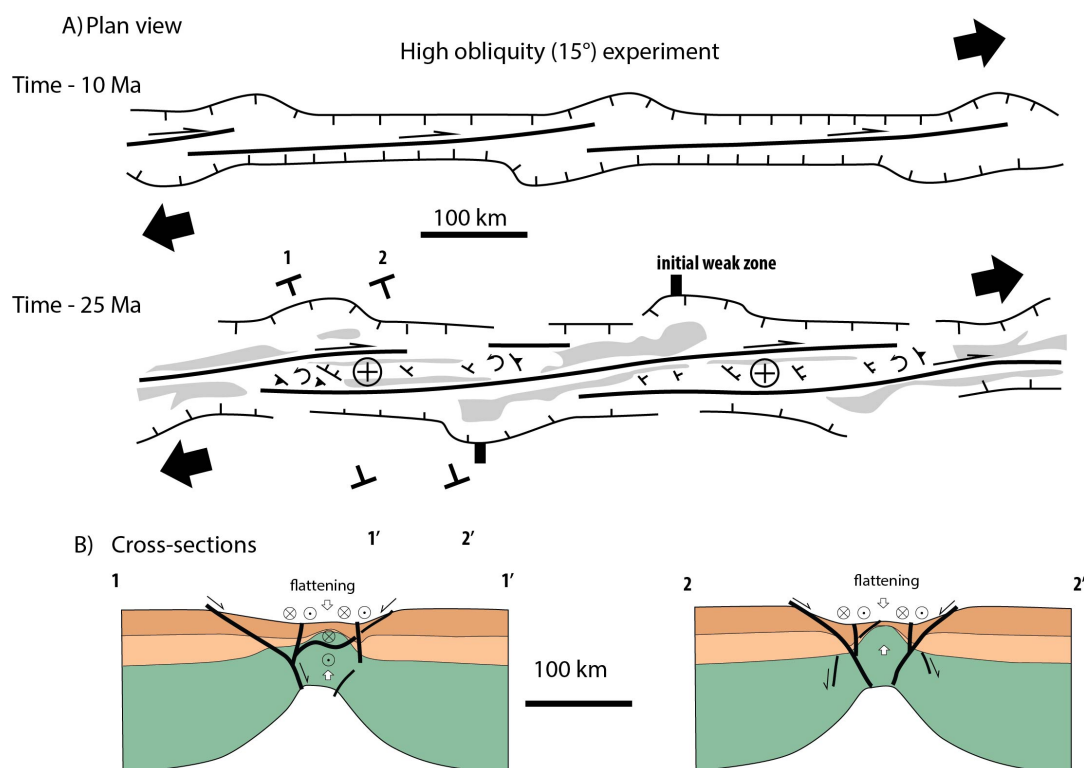
122
123   **Figure 3** : Sketch showing two steps (after 10 Myrs and 24 Myrs) of a 3D thermo-mechanical model of oblique rifting
124   in plan view (A) and cross-sections (B). Results are redrawn after (Jourdon et al., 2021) for the case of a highly oblique
125   experiment where extension is set with an angle of 15° with respect to the rift axis. Grey regions in (A) are basins
126   adjacent to uplifted domains (cross-circle symbol) associated with right-lateral strike-slip faults. Cross-sections (B)
127   depict the abrupt crustal thinning that occur perpendicular. Crustal thining is most visible for the lower crust and
128   produces the formation of an abrupt necking domain controlled by rift-parallel normal faults dipping towards the
129   center of the rift and right-lateral strike-slip faults.
130

131   **2. Geodynamics and STEP faulting in the Betics**

132   The onset of N-directed movement of Africa, by the Late Cretaceous-Paleogene, led to a Laramide-like contraction
133   from Morocco throughout Western Europe (Mouthereau et al., 2021). South of Iberia, in the Betic-Rif domain, the
134   closure of hyper-extended rift systems and oceanic basins of the Atlantic-Alpine Tethys resulted in the development
135   of a proto-Betic accretionary prism, likely largely submerged (Angrand and Mouthereau, 2021; Daudet et al., 2020;
136   Vergés and Fernàndez, 2012). By about 50 Ma, the acceleration of plate convergence led to the shortening of

137   continental rift and oceanic basins and topographic uplift all over Iberia (Daudet et al., 2020; Mouthereau et al., 2021,

138   2014; Rat et al., 2019; Vacherat et al., 2016; Waldner et al., 2021) associated with onset of continental rifting along the

139   Western European Rift (e.g. Mouthereau et al., 2021). 35 Ma ago, as Africa convergence slowed down, the western

140   Mediterranean sea opened accompanied by retreating slabs (Dewey, 1988; Dewey et al., 1989; Faccenna et al., 2014;

141   Jolivet and Faccenna, 2000; Rosenbaum et al., 2002). Subduction occurred mainly before 30 Ma as argued by age

142   constraints on high-pressure mineral assemblages (Romain Augier et al., 2005a; Bessière et al., 2021; Booth-Rea et

143   al., 2015; Gomez-Pugnaire and Fernandez-Soler, 1987; Platt and Vissers, 1989; Platt and Whitehouse, 1999) and has

144   been suggested to last until the mid-Miocene in the eastern Betics e.g. (Platt et al., 2013). The timing of formation of

145   the Alboran basin is constrained to 23 to 16 Ma by the oldest deposits found on Alboran basement and by the timing

146   of high-temperature metamorphic overprint and rapid cooling to shallow crustal temperature (Bessière et al., 2021;

147   Daudet et al., 2020; Janowski et al., 2017; Johnson et al., 1997; Platt et al., 2005; Sosson et al., 1998; Vázquez et al.,

148   2011; Zeck et al., 1992).

149   All kinematic reconstructions agree that extension results from the westward migration of the arc front and retreat of

150   the Alboran slab, well imaged below the Gibraltar arc as a steeply-dipping high-velocity anomaly (Bezada et al., 2013;

151   Heit et al., 2017; Mancilla et al., 2018, 2015a, 2015b; Palomeras et al., 2014; Spakman and Wortel, 2004; Villaseñor

152   et al., 2015). These reconstructions, however, differ according to the paleo-position of Alboran terrane, and hence to

153   the amount and vergence of subduction (Angrand and Mouthereau, 2021; Hinsbergen et al., 2014; Lonergan and

154   White, 1997; Romagny et al., 2020; Rosenbaum et al., 2002; Vergés and Fernàndez, 2012). Seismic tomography

155   reveals that slab detachment and tearing occur along the conjugate Alboran margins of the southern Betics and

156   northern Africa (Govers and Wortel, 2005; Heit et al., 2017; Mancilla et al., 2015a; Meighan et al., 2013; Spakman

157   and Wortel, 2004).

158   In **Fig. 4** we refer to the reconstruction of Angrand and Mouthereau (2021) that has the advantage of reconciling

159   previous western Mediterranean models (Romagny et al., 2020; Vergés & Fernàndez, 2012) with recent

160   thermochronological analyses in western Betics (Daudet et al., 2020) and other geological data (see compilation in

161   Mouthereau et al., 2021). This model accounts for the existence of an upper Cretaceous-Paleogene foreland basin that

162   formed adjacent to a proto-Betic orogen. In this reconstruction about 400 km of slab retreat is estimated since about

163   35 Ma (gray path, blue arrows in **Fig. 4**). It is worth noting that for Romagny et al. (2020) a similar amount (i.e. 400

164   km) is accommodated by back-arc extension of the Alboran crust, implying the same magnitude of displacement along

165   the STEP fault in the Betics. In the reconstruction of Angrand and Mouthereau (2021), however, crustal thinning in

166   Alboran basin is linked to delamination retrat of the Alboran lithospheric mantle towards the west. In such a model,

167   because of the decoupling between crust and mantle, the length of the delaminated slab resolved at depth in seismic

168   tomography, should not be simply translated into the amount of crustal extension in the Alboran domain. This further

169   implies the displacement across the STEP fault must be also less than 400 km. Daudet et al. (2020) suggested that an

170   extension of 110 km estimated from the restoration of low-angle detachment systems in the central and eastern Betics

171   (Martínez-Martínez et al., 2002) is likely to be a more accurate crustal estimate of the movement Alboran domain

172   rather than the total slab length.

173

174
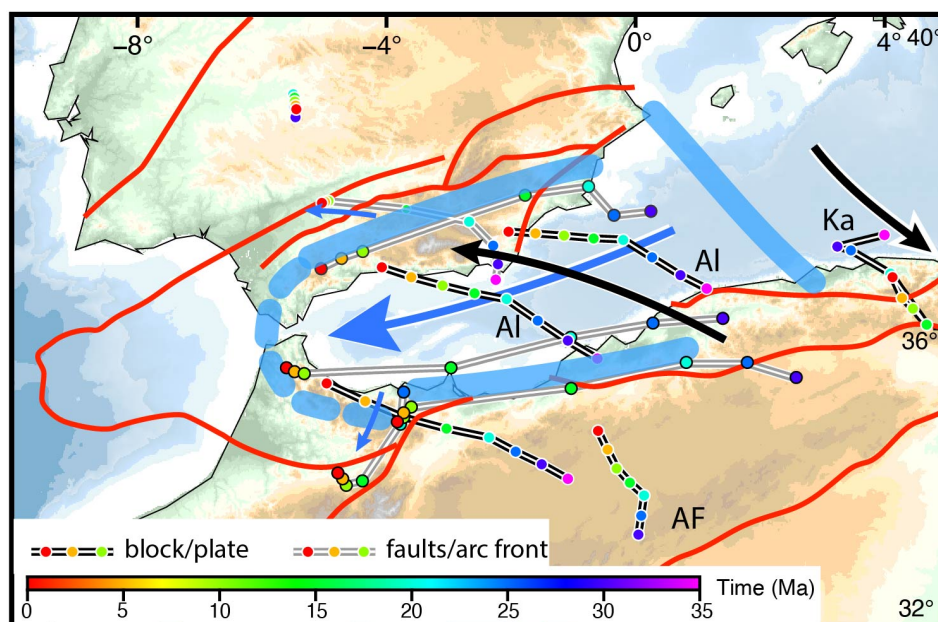
Figure 4: Kinematics of African plate (AF), Alboran (Al) and Kabylides (Ka) blocks with respect to fixed European plate since 35 Ma reconstructed after Angrand and Mouthereau (2021). Thick blue lines depicts the position of lithospheric tear faults (between Al and Europe and Africa) and transfer faults (between Al and Ka). Black arrows indicate the regional movement of Al and Ka with respect to Europe along black motion paths presented from 35 Ma to present. Grey motion paths refer to the motion of specific structures relative to Europe, including the motion of the arc front (thick blue dashed line) and faults in red. Dark blue arrow depicts the movement of the arc front due to retreating delamination towards the west.

3. Miocene extension in the eastern Betics

3.1 Relationships between domes and basins : from transtension and pure extension to late tectonic inversion

The most prominent extensional features in the eastern Betics are : 1) E-W elongated ranges that formed metamorphic domes with foliations bearing prominent E-W stretching lineations (**Fig. 5**; e.g. Sierra de los Filabres-Sierra Nevada, Sierra de Gador and the Sierra de las Estancias) and Serravallian-Tortonian sedimentary basins (Tabernas-Sorbas, Alpujarras, Almanzora and Huércal-Overa basins); 2) NNW-SSE/NW-SE normal fault systems and basins oblique to the domes such as the NW-SE trending Guadix-Baza and Alhabia basins (Galindo-Zaldivar et al., 2003; Martínez-Martínez and Azañón, 1997) (**Fig. 5**). They are described as asymmetric half grabens (Do Couto et al., 2014; Martínez-Martos et al., 2017; Pedrera et al., 2010, 2009) formed during the Upper Serravallian-Early Tortonian (Augier et al., 2005b; Augier et al., 2013; Meijninger and Vissers, 2006). Several of these NW-SE faults are active and cut across the metamorphic domes and the sedimentary basins (Augier et al., 2005a; Booth-Rea et al., 2004; Giaconia et al., 2012; Montenat and Ott d'Estevou, 1999).

In addition to these structures there are E-W right-lateral strike-slip faults that define structural corridors, like the Alpujarras corridor/basin between the Sierra de Gádor and the Sierra Nevada, and the Almanzora corridor/basin between the Sierra de los Filabres and Sierra de las Estancias (**Fig. 5**). The left-lateral Carboneras and Palomeras fault

198 system (Reicherter and Hübscher, 2006; Scotney et al., 2000) marks the tectonic limit with the Cabo de Gata volcanic

199 province (**Fig. 5**).

200 The domes are extension-related features interpreted either as 1) EW-metamorphic domes resulting from the

201 exhumation in the footwall of a regional W-directed extensional low-angle detachments, later folded during post-

202 Tortonian N-S contraction (e.g. Montenat & Ott d'Estevou, 1990; (Sanz de Galdeano and Vera, 1992; Sanz de

203 Galdeano and Alfaro, 2004; Martínez-Martínez et al., 2002; Martínez-Martos et al., 2017; Pedrera et al., 2010, 2007)

204 or 2) Miocene metamorphic domes formed by constrictional ductile strain regime accompaniying W-directed

205 stretching of the Alboran domain and trench retreat, with limited overprint by the Tortonian contraction ca. 8 Ma

206 (Augier et al., 2013; Augier et al., 2005; Augier et al., 2005b; Galindo-Zaldivar et al., 2015; Jolivet et al., 2021b;

207 Martínez-Martínez et al., 2002). Low-temperature constraints from the Nevado-Filabride and Alpujarride complexes

208 confirm the west-directed exhumation of the basement that occurred progressively from the Sierra de los Filabres at

209 ~13-11 Ma (Serravallian) in the East to the Sierra Nevada at 8-6 Ma (Tortonian) in the West (Clark and Dempster,

210 2009; Janowski et al., 2017; Johnson et al., 1997; Platt et al., 2005; Reinhardt et al., 2007; Vázquez et al., 2011).

211

212
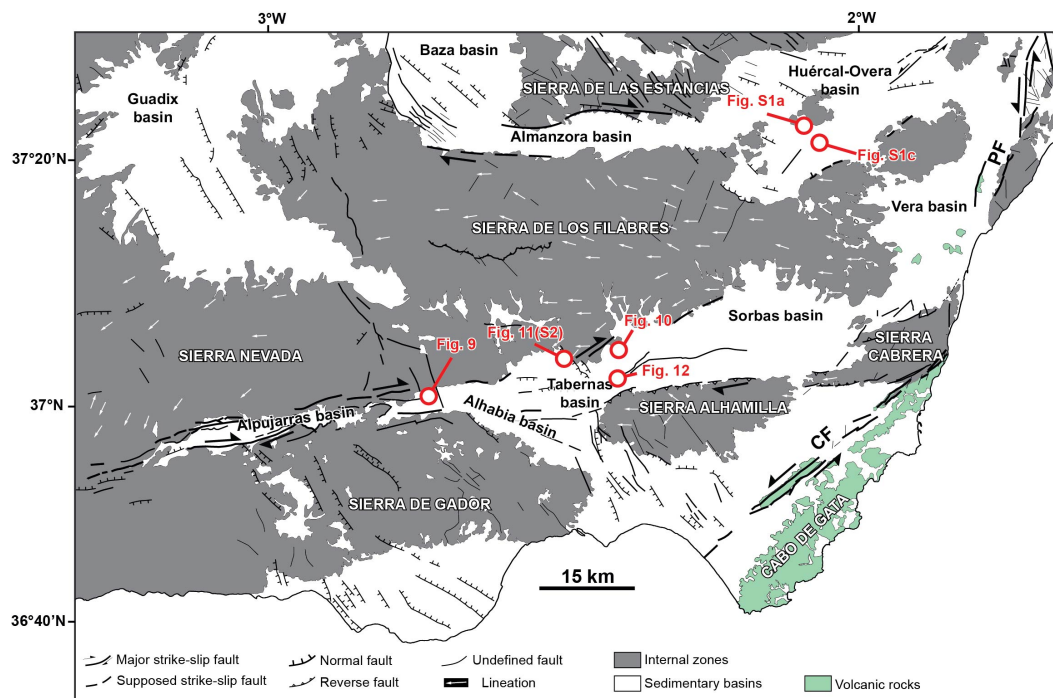
Figure 5 : Tectonic map of the eastern Betics showing the main structural elements in black after Augier et al. (2005)
214 and Do Couto (2014). CF: Carboneras Fault; PF : Palomeras Fault.

215

216 Tectonic models for the formation of Neogene intramontane sedimentary basins vary depending on the prevailing

217 tectonic regime. EW-directed basins have been early described as pull-apart basins (e.g Alpujarran corridor) (Sanz de

218 Galdeano et al., 1985). Structural analyses then led to re-interpret these structures as transfer zones resulting from

219   differential extension between exhuming core-complexes (and detachment systems) since the Serravallian (13-11 Ma)
220   later refolded during Tortonian (9-8 Ma) compression (Martínez-Martínez et al., 2006). In support to the dominant
221   regional compressional stress regime, Martínez-Martos et al. (2017) proposed the E-W depressions are related to the
222   tectonic reactivation of crustal weakness zone as dextral strike-slip faults in a counterclockwise rotation,
223   accommodating part of the the N-S shortening. There are evidence that at the end of the Tortonian a regional uplift
224   occurred, rising the remnants of late Tortonian marine platform, 7.2 Ma in age, to 1600 m above sea level in the Sierra
225   de Gádor (Braga et al., 2003; Janowski et al., 2017), coincidently with the onset of contraction in the Sierra Alhamilla
226   and Sierra de los Filabres (e.g. Do Couto et al., 2014), in the Alboran domain (e.g. (Martínez-García et al., 2017) and
227   on the margins of the eastern Betic (Giaconia et al., 2013).

228   Based on the prevalence in some EW-trending basins, like the Huércal-Overa basin, of EW-trending normal faults,
229   these basins have alternatively been interpreted as resulting from late exhumation stage of the domes, possibly as soon
230   as the Serravallian, but mostly after the early Tortonian (syn-sedimentary faulting) (Augier et al., 2013; Romain Augier
231   et al., 2005b; Meijninger and Vissers, 2006). The NW-SE/NNW-SSE sedimentary basins (Guadix, Baza, Alhabia;
232   **Figs. 5**), in contrast, are extensional basins formed parallel to the direction of the regional compression (Sanz de
233   Galdeano and Vera, 1992; Larouzière et al., 1988). E-W strike-slip corridors, aligned in the direction of the domes,
234   and NW-SE normal faulting patterns are both key features consistent with predictions from models of oblique
235   extension at transform margin (**Fig. 3**). Yet, based on existing structural and tectonic syntheses a clear temporal
236   relationships between E-W ductile stretching in the domes and ~~transcurrent~~ deformation is not established (**Fig. 5**).

238   **3.2 ~~Are~~ the Tortonian rift-related subsidence consistent with oblique extension ?**
239   The stratigraphic architecture and depositional evolution of Tortonian intramontane basins provides first-order
240   informations on the distribution of crustal thinning. ~~The oldest sediments deposited unconformably on the Paleozoic-~~
241   ~~Triassic basement are red alluvial conglomerates and deltaic series dated from Serravallian to lower Tortonian (~11-~~
242   ~~9 Ma)~~ (**Fig. 6a**). These continental deposits are thicker and well exposed on the flanks of the Almanzora basin and on
243   the northern Huércal-Overa basin (HOB), compared to the Alpujarras Corridor (AC) and Tabernas basin (TB) (**Figs.
244   6 and 7a**; Augier et al., 2013; Pedrera et al., 2010, 2007; Poisson et al., 1996).

245   Paleogeographic reconstructions indicate they were deposited on a large emerged domain, stretching from Huercal-
246   Overa to Granada, in the West and in Tabernas, to the South (Braga et al., 2003). Sourced from the Nevado-Filabride
247   metamorphic complex (Hodgson and Haughton, 2004; Kleverlaan, 1989; Meijninger and Vissers, 2006; Pedrera et
248   al., 2010, 2007; Pickering et al., 2001; Weijermars et al., 1985) these deposits mark the onset of surface exhumation
249   of the Sierra de Las Estancias and Sierra de Los Filabres.

250   During this intial stage, HOB is the most subsident basin (**Figs. 6b, 7a and 7b**), accumulating sediments at rates of
251   400 m/Ma while rates are 140-180 m/Ma in the Tabernas basin (**Fig. 6b**) (Augier, 2005). Higher subsidence in the
252   HOB, which also started earlier than in other basins, suggests extension occurred originally to the North associated
253   with the exhumation of the Sierra de Las Estancias. Basal continental conglomerates are overlain by grey coarse-
254   grained Tortonian sandstones found occasionally, e.g. in the Almanzora basin, intercalated with marine marls (**Figure

255   **6a**). They are topped by mid-Tortonian bioclastic calcarenite and coral reefs (Braga et al., 2003; Martin et al., 1989;

256   Pedrera et al., 2007).

257   During the same interval, TB recorded the deposition of 300 to 400 m of coarse to medium-grained deltaic marine

258   clastics overlying unconformably the lowermost red series (**Fig. 6a**). These sediments pass upwards, e.g. in TB, to

259   deeper marine 1200 m-thick turbiditic and marls series intercalated with regional-scale megabeds, revealing the onset

260   of rapid tectonic subsidence (Haughton, 1994; Kleverlaan, 1989, 1987; Pickering et al., 2001; Weijermars et al., 1985).

261   Details of depositional architecture of the Tortonian suggest that part of this subsidence evolution was controlled by

262   E-W directed strike-slip faults (Haughton, 2000) under transtensional strain.

263   The transition from continental to deep marine sedimentary environments (water depth of 400-600 m according to

264   Poisson et al., 1999) witnesses the rapid rift-related tectonic subsidence achieved during the upper Tortonian times

265   (~9 Ma; **Figs. 6** and **7c**) (Romain Augier et al., 2005b; Montenat and Ott d'Estevou, 1992; Weijermars et al., 1985).

266   At around 8 Ma, accumulation rates drop by a factor of two to 200 m/Ma in HOB and 70 m/Ma in TB, revealing a

267   marked reduction in subsidence. Subsidence then became negative as basement uplifted from around 7 Ma (**Figs. 6b**

268   and **7d**) in both TB and HOB.

269

270
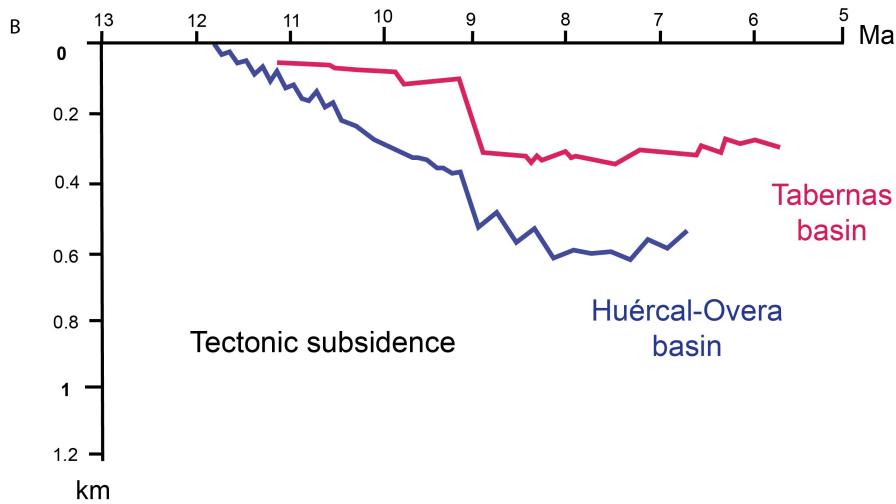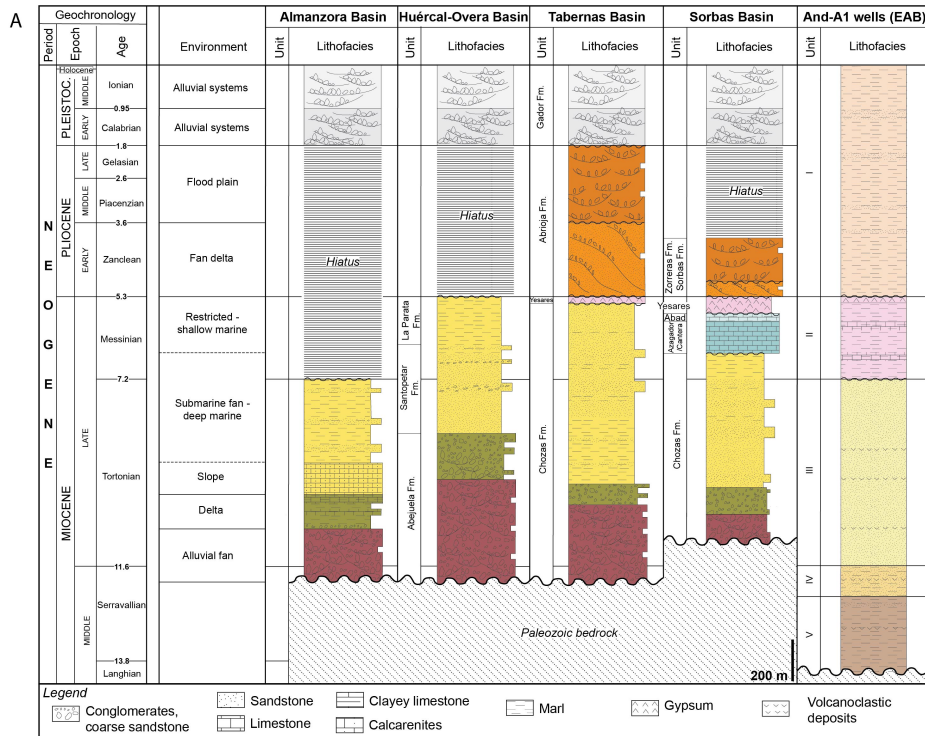
271
272 **Figure 6** : Stratigraphic evolution and lithologies of intramontane basins in the eastern Betics and offshore A1 well.
273 (a) Neogene stratigraphy and basin-fill correlation in the Almanzora and Huercal-Overa basins (Mora, 1993), Tabernas
274 basin (Hodgson and Haughton, 2004; Kleverlaan, 1989; Pickering et al., 2001) and Sorbas basin (Fortuin and
275 Krijgsman, 2003; Martín and Braga, 1994; Riding et al., 1998). Middle Miocene sedimentary environments in the
276 Alboran Sea are after (Comas et al., 1992). (a) Neogene tectonic subsidence evolution for Tabernas basin and Huércal-
277 Overa basin are from (Augier, 2004). The curves are obtained from backstripping techniques incorporating local
278 eustatic and paleobathymetric corrections.

279

280 The geometry of the Almanzora (Pedrera et al., 2009), Sorbas (e.g. Do Couto et al., 2014) and Huércal-Overa basin

281 basins (Pedrera et al., 2010) inferred from gravity measurements indicate that these basins are asymmetrical and

282 deepening southwards (**Fig. 5**). This sediment infill pattern recalls the formation of asymmetrical basins predicted by

283 numerical models of flexural strike-slip basins (Neuharth et al., 2021). According to this model, the asymmetry

284 observed should reflect the developement of strike-slip basins loaded by sediments originated from the North. In

285 addition, a larger subsidence in HOB is an indication of abrupt crustal thinning to the south of Sierra de las Estancias

286 where the crustal thickness of 35 km is the largest (**Fig. 2**). Therefore, at least the Serravallian-Tortonian infill patterns

287 agree with oblique extension.

288
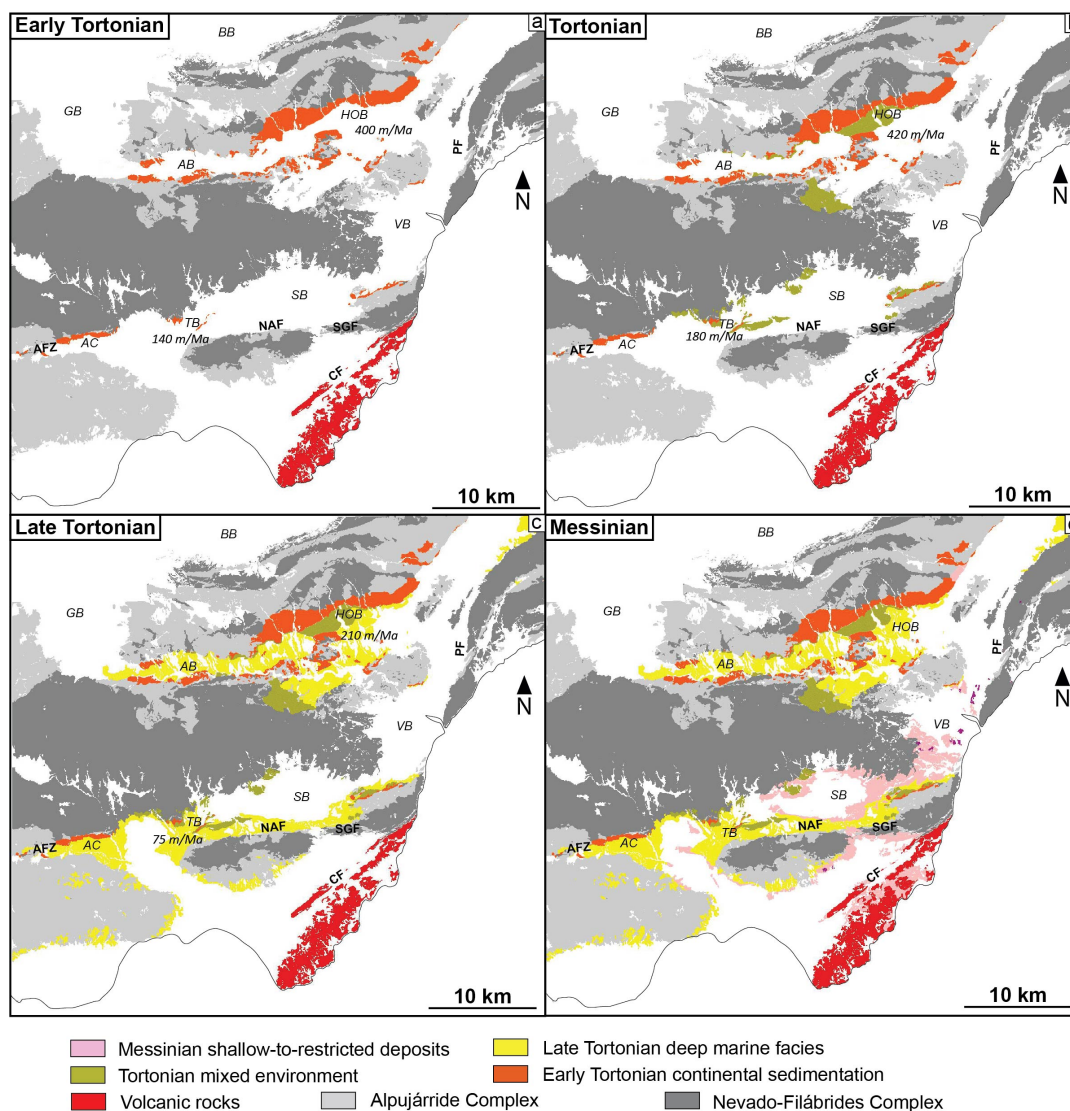
Figure 7: Distribution of (a) lower Tortonian, (b) Tortonian, (c) upper Tortonian and (d) Messinian deposits based on geological mapping of the different basins. CF: Carboneras Fault; PF : Palomeras Fault; SGF: South Gafarillo fault; NAF: North Alhamilla fault; AFZ: Alpujarras fault zone; BB: Baza basin; GB: Guadix basin; AB: Almanzora basin; HOB: Huercal-Overa basin; VB: Vera basin; SB: Sorbas basin; TB: Tabernas basin; AC: Alpujarras corridor.

4. Brittle faulting : pure extension versus transtensional deformation in Neogene basins

4.1. Tectonic regime in the eastern Betics

Figure 8 presents a compilation of 112 fault slip data inversion previously analysed in the eastern Betics combined with new measurements conducted in the Alpujarras Corridor and in the Tabernas basin (**Table S1**). Most faults are syn-Tortonian or cut through the Tortonian. This compilation emphasizes a regional trend of σ3 stress axes oriented

300 NNE-SSW (N20°E) with subordinate σ3 oriented E-W. In details, this well-defined regional horizontal extension

301 reflects a combination of pure normal faulting regime (σ2 horizontal and oriented NW-SE/WNW-ESE) and strike-

302 slip faulting regime (σ2 vertical to steeply-dipping and σ1 horizontal an striking NNW-SSE). N-S to NW-SE

303 compression is also reported in the HOB associated with incipient synform and depocenter which is dated to the lower

304 Tortonian coeval with the prominent EW/WSW-ENE extension (e.g. Pedrera et al., 2010).

305 We describe below, based on a selection of oucrops in the vicinity of the contact between Tortonian basins and major

306 metamorphic domes, the expression of EW and NW-SE extensional faulting in the field. We then discuss how they

307 are linked to the regional stress regimes.

308
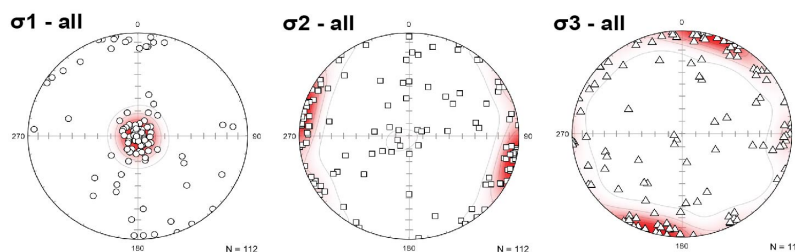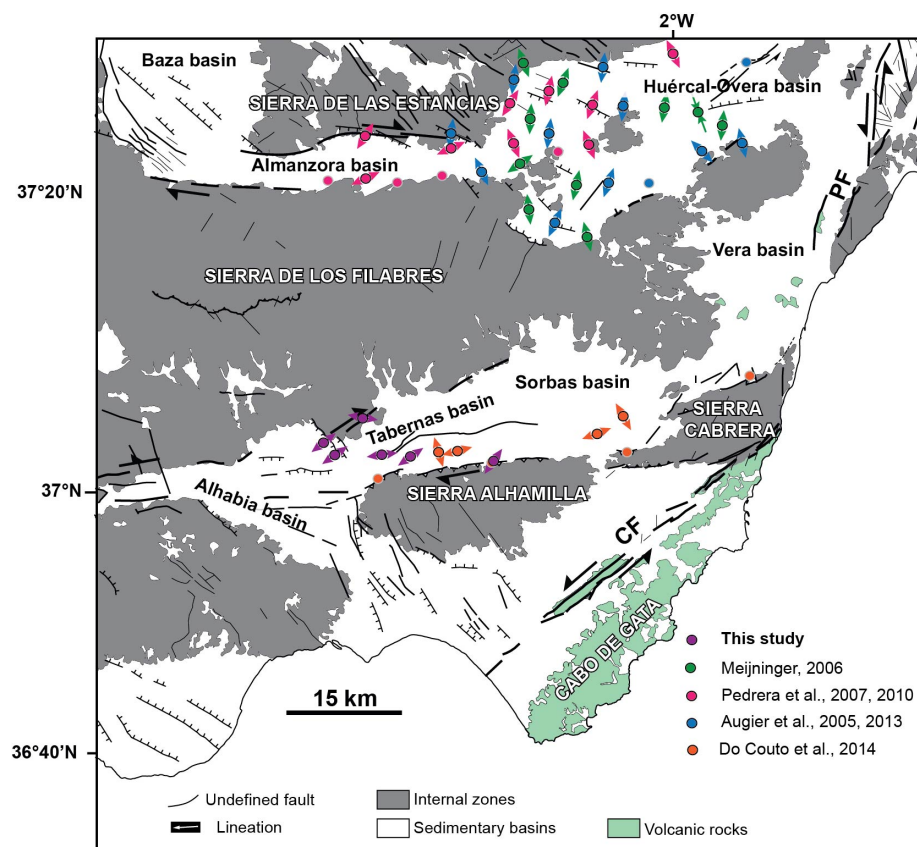
309

310 **Figure 8**: Synthesis of stress regimes resolved from fault slip data inversion in Tortonian basins. Color-coded circles
311 with arrows depict tectonic sites where extension (given as arrows) is horizontal (pure extensional or strike-slip stress
312 regimes). Sites where reverse tectonic regimes prevail are shown as circles highlighted in grey. Below, stereoplots of
313 paleostresses σ1, σ2 and σ3 show a compilation of all brittle tectonic regimes extracted from Table S1. Collectively
314 they define a prominent extension oriented NNE-SSW with a subordinate E-W-striking extension. CF: Carboneras
315 Fault; PF : Palomeras Fault.
316

4.1 EW-directed faulting: evidence for pre-Tortonian oblique extension ?

318 In Tortonian intramontane basins, one of the main set of faults is represented by E-W-directed faults, including ENE-
319 WSW to ESE-WNW sets. North of the Alpujarras Corridor (AC), 3 km to the NE of Canjáyar, the contact between
320 the basal Tortonian conglomerates and the series of Alpujarride complex is exposed in the Rambla de Tices. It is
321 shaped by a 2-meter thick fault zone (**Figs. 9a,b**) striking N100°E, which has a normal sense of slip with a right-lateral
322 strike-slip component (**Fig. 9c**). It consists of cataclastic breccias and sheared blocks (boudins) of the host rocks (**Fig.**
323 **9d**). This major fault is found along the 65 km-long Alpujarras fault zone described by Martínez-Martínez (2006) as
324 a major strike-slip dextral transfer zone south of the Sierra Nevada that accommodates both WSW-extension and dextral
325 movement. It is mechanically consistent with NE-SW/ENE-WSW extension under a strike-slip regime as resolved
326 nearby along the same faults system (Martínez-Martínez, 2006). **Fig. 9** indicates the fault is parallel to the basal
327 Tortonian series but cuts across the Alpujarride complex. In the HOB, on the southern flank of the Sierra Limaria, the
328 unconformity between the lower Tortonian red conglomerates and the Alpujarride units (Rambla de Cordoba, 2km
329 NW Arboleas, **Figs. S1a, b**) is found reactivated as a normal fault with a dextral shear component.

330 To the North of TB, a large morphological surface presents a rare exposure of the micaschist basement of the Nevado-
331 Filabrides complex allowing the study of deformation on the southern flank of the Sierra de los Filabres (**Fig. 10**). The
332 deformed NF series shapes a kilometric-size antiform with axial planar surface dipping towards the North. The steeply-
333 dipping cleavages directed NE-SW on its southern flank are deformed by numerous dextral shear zones with lengths
334 ranging from 100 m to less than 5 m (**Fig. 10b, c**). In addition to isoclinal folds parallel to the main foliation that are
335 clearly associated to an early stage of ductile EW-stretching, we recognize close to the strike-slip shear zones, steeply-
336 dipping metric-size open to tight folds inclined to the NE (**Fig. 10d**). To the south, Tortonian conglomerates are
337 overlying unconformably the folded NF foliation. This stratigraphic relationships and the average low dip of Tortonian
338 strata (20°SE) indicate that strike-slip deformation occurred before the deposition of Tortonian conglomerates and
339 after the tilting of the NF foliation (see cross section in **Fig. 10a**). This argues that the transition from W-directed
340 ductile extension in the metamorphic domes known to have started in the Burdigalian and the right-lateral strike-slip
341 faulting occurred around the Langhian-Serravallian (13-14 Ma). This interval is often considered to mark the transition
342 from ductile to brittle extension (e.g. Augier et al., 2013). Because strike-slip faulting postdates folding of the NF
343 foliation, and are consistent with WSW-ENE oblique extension, we suggest that the Sierra de los Filabres metamorphic
344 dome formed in a transtensional strain regime. This hypothesis conforms with prediction of transtension at the tip of
345 the STEP fault (Le Pourhiet et al., 2012) and with model of oblique extension (see **Fig. 3**).
346
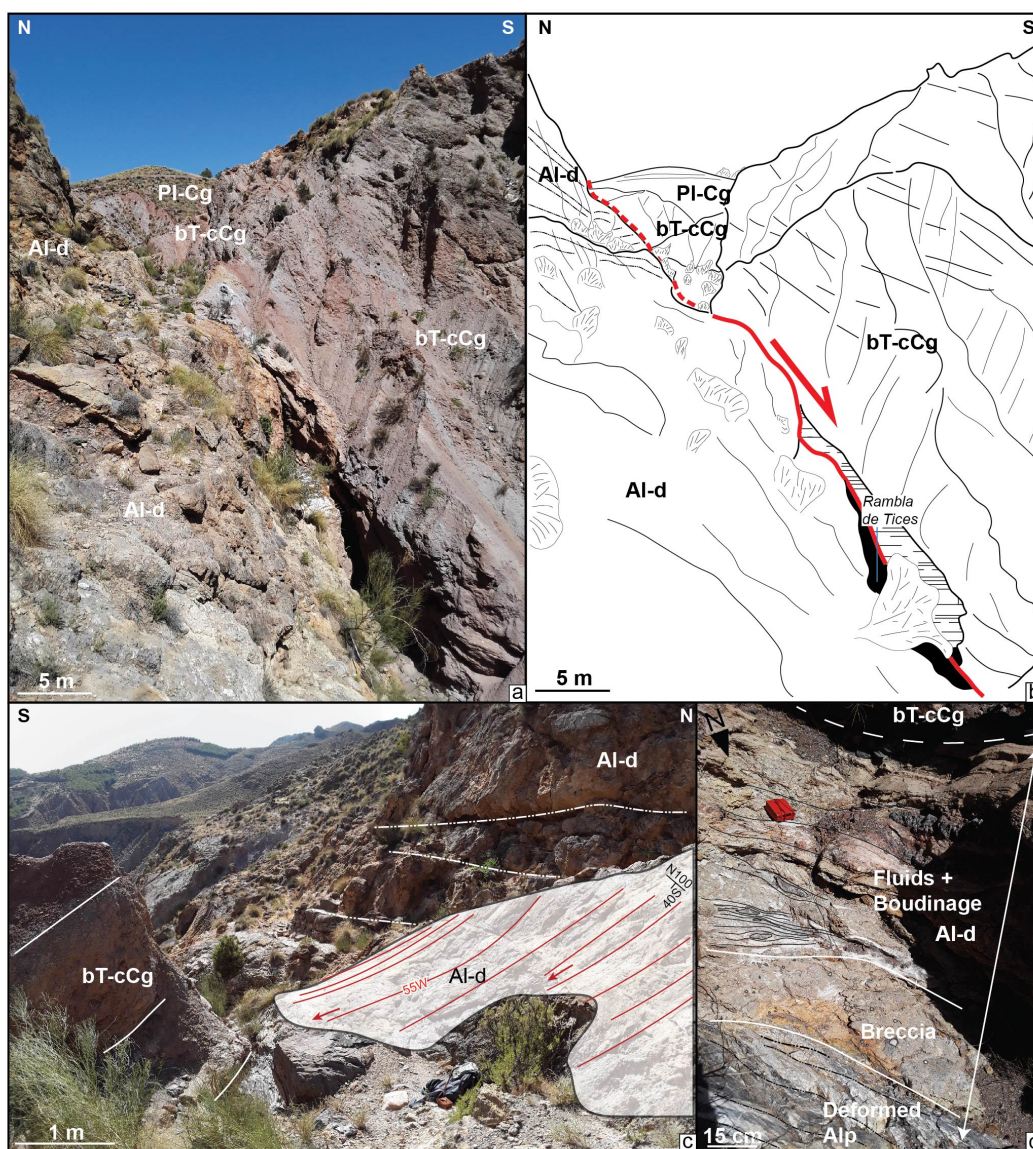
Figure 9. (a) and (b) Fault zone at the contact between the Tortonian basal conglomerates and the series of the Alpujarride complex south of AC (Rambla de Tices, see **Fig. 5** for location). (c) slikenslides on the fault zone reveasl a normal sense of slip with right-lateral strike-slip component found in association with (d) cataclastic breccias, sheared boudins of metamorphic and sedimentary rocks. Al-d: Alpujarride dolomites; bT-cCg: basal Tortonian continental Conglomerates; Pl-Cg: Pliocene Conglomerates. Coordinates 37.031944°N/-2.716274°E.

4.1.2. NW-SE-directed normal faulting

A second set is represented by NW-SE directed normal faults (**Fig. 8**). They are found, for instance, on the border of the NW-SE Alhabia basin, where they cut across the basement and interrupt the westward continuity of the Sierra de

357   los Filabres. One major fault zone of this system is well exposed in the Arroyo del Verdelecho, 7 km to the west of
358   Tabernas, on the eastern border of the Alhabia basin (**Figs. 11 and S2**). From a regional point of view this large NW-
359   SE fault zone controls the deepening of the Tortonian basin and the position of Pliocene depocenter in its hangingwall,
360   towards the West. NW-SE normal faults also cut across the lower Tortonian conglomerates in the hanginwall but their
361   throw diminishes upward in the upper Tortonian margin sediments, suggesting fault activity during the late Tortonian
362   (**Fig. 11**). One major fault zone is outlined by cataclastic breccias made of marbles originated from the exhumed
363   Alpujarride complex in the Sierra de los Filabres (**Fig. S2**).
364   South of HOB (south of Arboleas), NW-SE faults are seen cutting through the late Tortonian sands and marls series,
365   indicating that NE-SW extension is at least Tortonian (**Figs. S1c, d**).
366
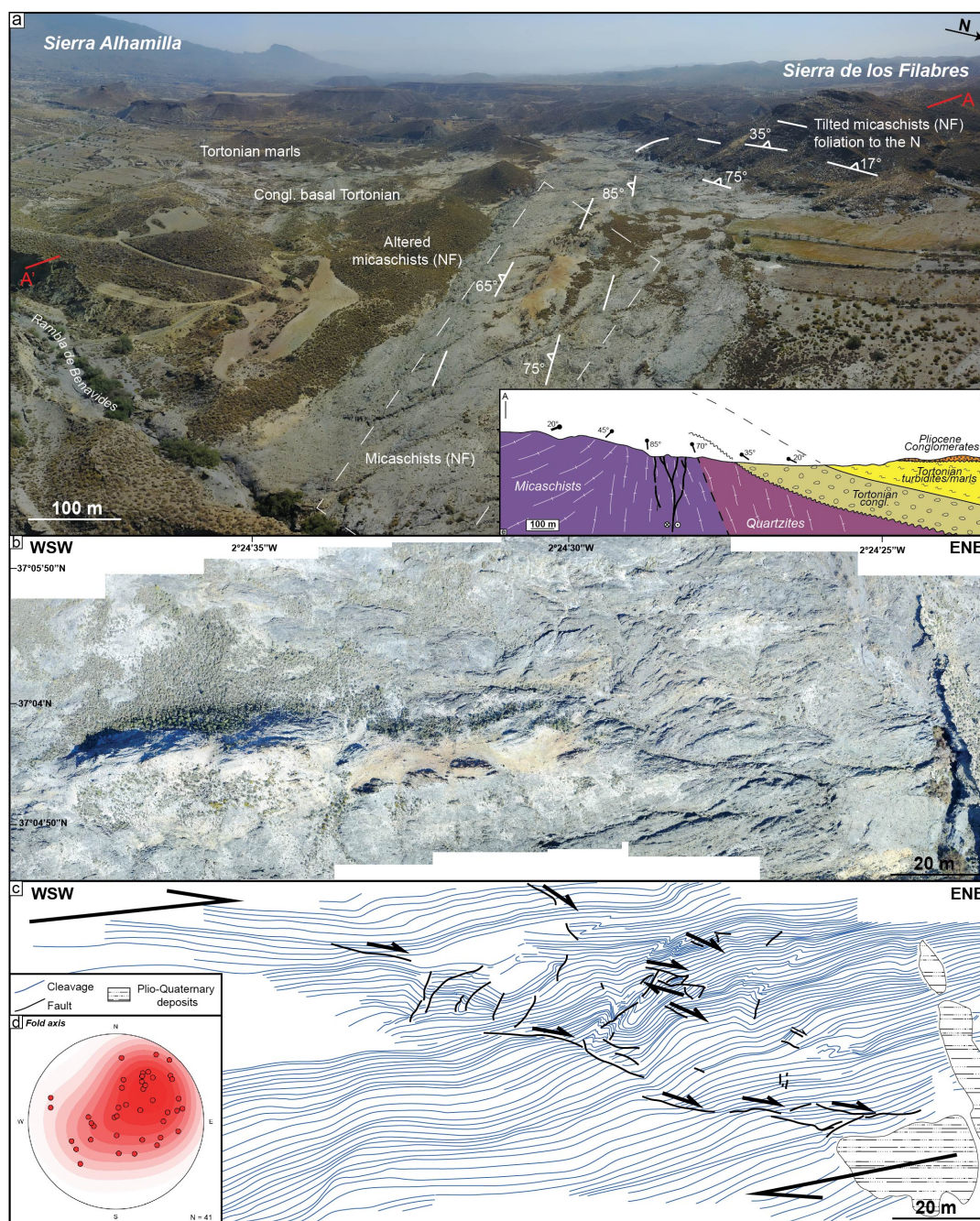
Figure 10 : (**a**) Drone view taken in the SSW direction of the southern flank of the Sierra de los Filabres at the contact with the Tabernas basin (see Figure 5 for location). Local folding of the micaschist is apparent in the right where the foliation is striking NNE-SSW and is dipping ~25°E whereas it is vertical and striking SW-NE in the center of the studied area forming paleosurface. Local cross section highlights the unconformable contact between the Tortonian conglomerates and overlying on the basement. (**b**) High-resolution drone images of the paleosurface and (**c**) line-

373 drawing of the foliation revealing secondary folding (see (**d**) stereoplot of fold axes inclined to the NE) and dextral
374 shear zones. Coordinates 37.082777°N/-2.410544°E.
375

376

377
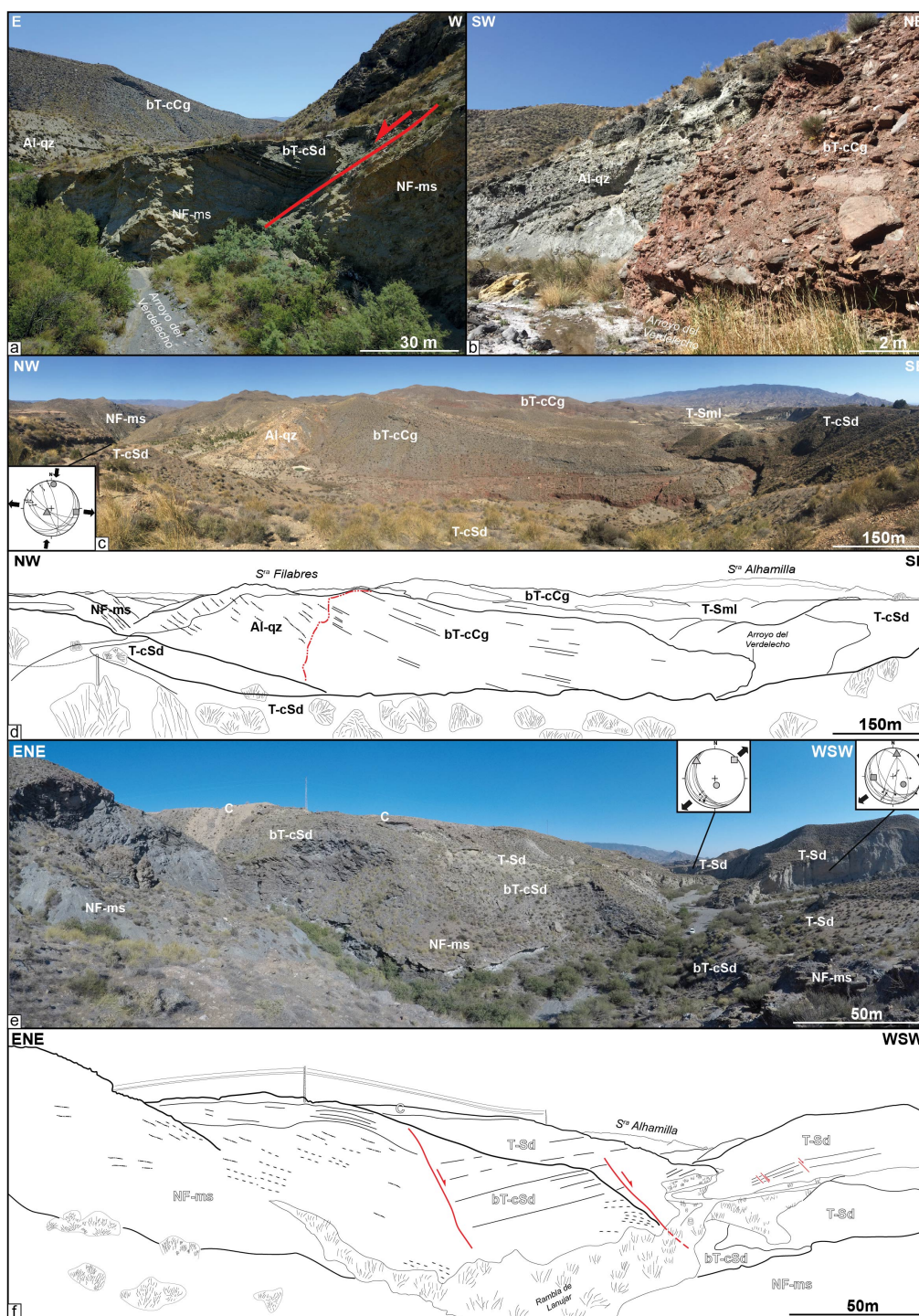
379   **Figure 11** : (**a**) Field photographs of a NW-SE normal fault at the contact between the Nevado-Filabride micaschists
380   (footwall) and Tortonian sediments (hanginwall). (**b**) Stratigraphic contact between grey and red basal Tortonian
381   continental conglomerates. These thick Tortonian series rest conformably on the Alpjuarride complex (**c**, **d**).
382   Coordinates 37.059507°N/-2.478386°E. (**e, f**) NW-SE Normal faults cutting across the NF micaschists basement.
383   These faults that also affetc the early Tortonian deposits are sealed by late Tortonian deposits and are therefore syn-
384   depositional. See Figure 5 for location. Al-qz: Alpujarride quartzites; NF-ms: Nevado-Filabride micaschists; bT-cCg:
385   basal Tortonian continental Conglomerates; bT-cSd: basal Tortonian continental Sandstones; T-cSd: Tortonian coarse
386   Sandstones; T-Sd: Tortonian Sandstones; T-Sml: Tortonian Sandstones-marls; C: calcretes. Coordinates
387   37.061279°N/-2.490309°E. Paleostress orientations are in Table S1.
388

389   Both fault slip data and our own observations argue for a regional pre-Tortonian and syn-early Tortonian NNE-

390   directed extension. This direction of extension is also found associated with less well-developed strike-slip regimes

391   (**Fig. 8**). It is consistent with the D1-D2 phase of brittle deformation found in HOB (Augier et al., 2013). The fact that

392   extension and strike-slip regimes occurred synchronously, or overlap rapidly in time, supports the view that they

393   reflect the same large-scale tectonic setting. The reason why strike-slip faulting is less apparent in the field than

394   expected in models in **Fig. 3** is likely to reflect the fact that oblique extension is not fully partitioned between normal

395   and strike-slip components and is actually distributed along oblique structures. Moreover, where strike-slip faults are

396   found they are associated with narrow corridor basins or near the contact betwen the cover and basement but not in

397   the center of HOB or TB. The NNE-SSW to NW-SE faults appear to postdate the deposition of the early Tortonian

398   red conglomerates and is synchronous with the deposition of marine Tortonian series (**Fig. 12**). These normal faults

399   currently form half-graben filled with Plio-Quaternary deposits (Guadix, Baza, Alhabia) and are active today. But the

400   importance of extension-related brittle deformation over brittle compression decreases easttwards. Indeed, a late brittle

401   compressional event oriented roughly N-S is described in the literature as a D3 brittle event (e.g. in HOB) associated

402   with reverse and strike-slip faults (Augier et al., 2013). The post-late Tortonian shortening is seen responsible for fold

403   amplification and reverse faulting on the northern limb of Sierra de Alhamilla and Sierra de los Filabres, and locally

404   in the eastern part of the HOB near the termination of left-lateral strike-slip faulting evolution of the Alhama de Murcia

405   fault (**Fig. 8**).
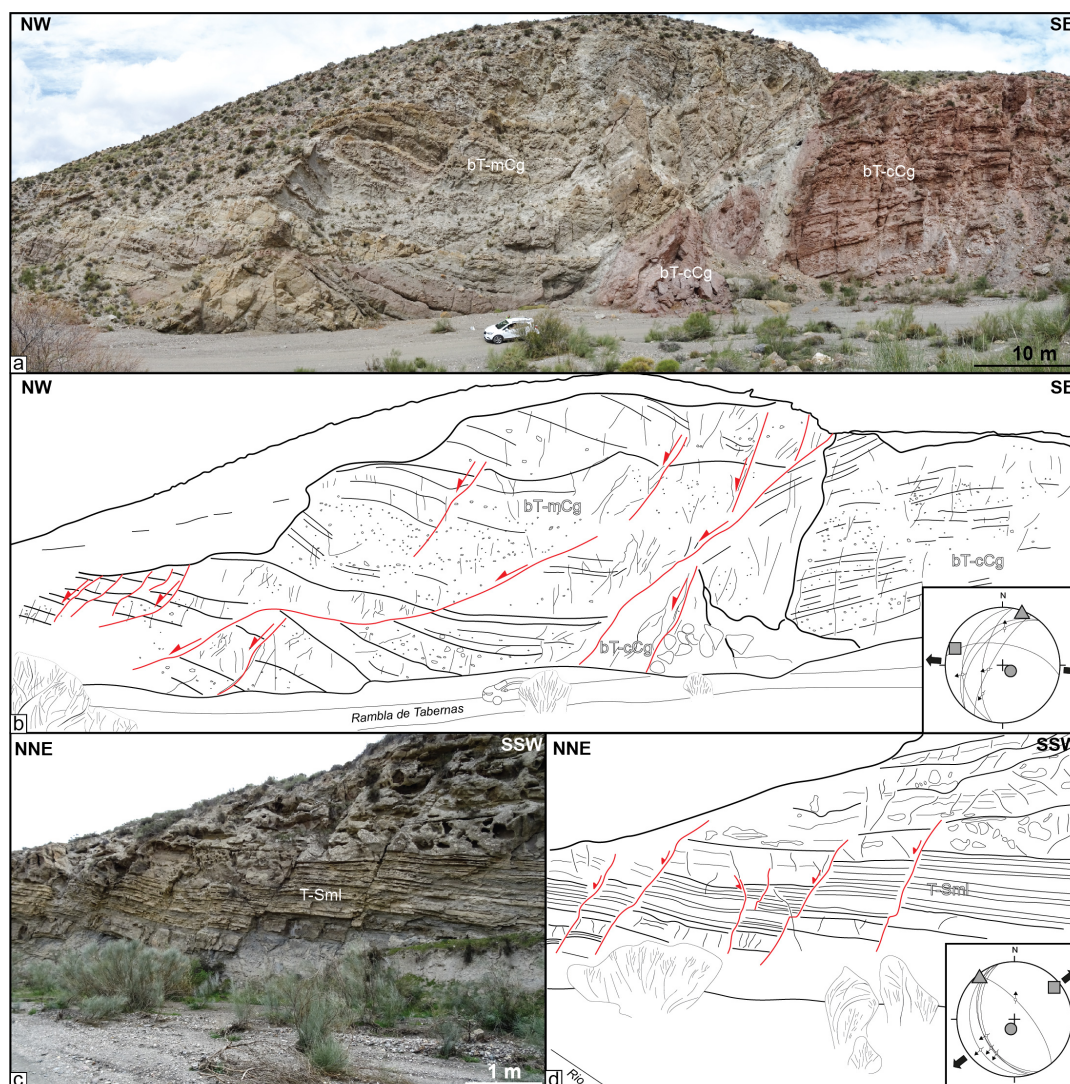
Figure 12: (**a, b**) N-S to NNE-SSW-oriented normal to dextral faults affecting the basal Tortonian continental conglomerates (bT-cCg) and marine conglomerates (bT-mCg) (Rambla de Tabernas). They form a long and tight E-W anticlinal crosses the Tabernas basin (see Figure 5 for location). (**c, d**) Several normal faults observed in Tortonian sandstones and marls (T-Sml). They are mostly oriented NNW-SSE. Coordinates 37.041648°N/-2.399318°E. Paleostress orientations are in Table S1.

5. N-S crustal-scale section across the oblique/transform margin of Alboran basin

To examine further the structural relationships between extension and strike-slip faulting across the Alboran margin, we explore 2D multichannel seismic lines acquired during the MARSIBAL 1-06 cruise (Comas and MARSIBAL1-06 Scientific Party, 2007) and ESCI cruises (Comas et al., 1995) across the Eastern Alboran basin (EAB). The studied seismic dataset consists of ~300 km and are deep-penetration multichannel seismic reflection studies (12 s two-way travel time - TWTT). Here, we study two lines namely MSB08 and MSB07 (see location in **Fig. 1**). For stratigraphic

418 and structural correlations between the studied seismic lines, we used the Andalucia-A1 well (**Fig. 6a**) and results

419 from ODP 977 and 978 legs (see location in **Fig. 1**). MSB08 is striking N70°E, slightly oblique to the shoreline. It is

420 close, and runs parallel, to TM08 line of (Peña et al., 2018). It is calibrated by Andalucia-A1 well and ESCI-Alb1 line

421 (Comas et al., 1995). Line MSB07 stretches in the N-S direction between the EAB in Spain and SAB to the north of

422 Morocco parallel to line TM09 (Peña et al., 2018) and crosscuts line ESCI Alb2b presented in Comas et al. (1995)

423 and Booth-Rea et al. (2007) (**Fig. 1**).

424

425 **5.1 Offshore structures and stratigraphic architecture**

426 The Carboneras Fault is well imaged north of MSB07 (**Fig. 13**). It forms a positive crustal-scale antiformal flower

427 structure related to left-lateral strike-slip faulting that involves a Moho depth variation between 12 s to 9-8 s TWT

428 after Gomez de la Peña et al. (2018). It separates a thin continental crust to the North (25-20 km; **Fig. 2**), from the

429 magmatic calc-alkaline arc crust of the EAB with a thickness of 18 km in the south (Booth-Rea et al., 2007, 2018;

430 Gomez de la Peña et al., 2018, 2020a).

431
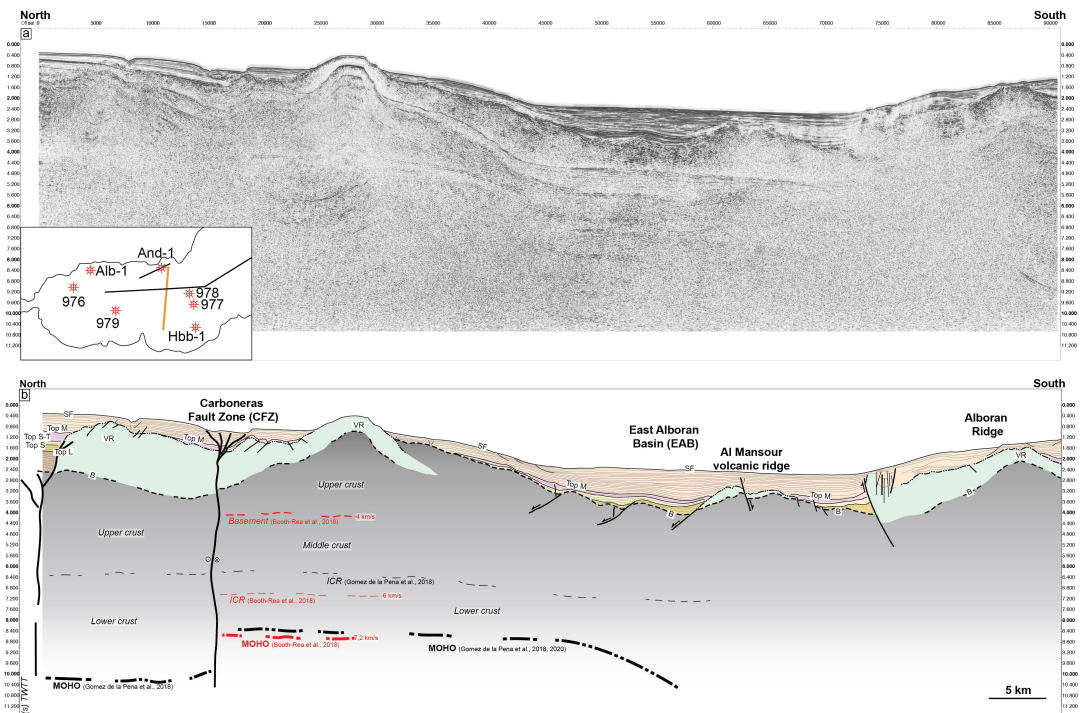
432

433 **Figure 13** : Seismic reflection line MSB07 (location on **Fig. 1**). Discontinuous intracrustal reflectors (ICR) imaged
434 between 3 and 6.5 s TWT, have been interpreted as mylonitic zones within the metamorphic basement (Carbonell et
435 al., 1998; García-Dueñas et al., 1994; Gomez de la Peña et al., 2018). VR: Volcanic Ridge; B: Acoustic basement;
436 Top L : Top Langian; Top S: Top Serravallian; Top S-T: top Serravallian-Tortonian; Top M: Top Messinian; SF:
437 Seafloor.
438
439

440

441   Reflection seismic data (**Figs. 13, 14, 15**) collectively show a relatively well stratified crust, corresponding to the

442   sediment cover, down to 2.4-4 s TWT which outlines the acoustic basement with high reflectivity (B). Locally, the

443   top basement reflector coincides with erosional palaeo-relief or high angle normal faults bounding basement highs.

444   These faults are oriented mostly NW-SE to NE-SW and cut across the basement. We recognized on seismic images

445   magmatic additions in the continental crust that are shaped by volcanic edifices exposed on the seafloor (e.g. Chella

446   Bank) or slightly buried (Alboran Ridge) outlined by symmetric downlaps and onlaps of sediments. These

447   constructions form topographic highs such as the Chella Bank on the MSB08 line (**Fig. 14**), the Alboran Ridge on the

448   MSB07 line (**Fig. 13**) and the Maimonides Ridge on the ESCI-Alb2b line (**Fig. 15**). All the reflectors corresponding

449   to layers as old as Tortonian are onlapping against the volcanic ridges confirming that the volcanic activity occurred

450   during the middle to late Miocene times, which is otherwise shown by Duggen et al. (2008). Some reflectors up to the

451   top Messinian (top M) onlap onto the volcanic ridges probably as a result of Pliocene uplift.

452   The stratigraphy offshore, on the continental crustal domain, is defined by the recognition of five seismic stratigraphic

453   units in Andalucía-A1 well (Jurado and Comas, 1992) labeled I-V from top to base (**Figs 6** and **16**) and separated by

454   unconformities. The seismostratigraphic units I to V vary in thickness (**Fig. 16**) and their architecture is conditioned

455   by the occurrence of basement highs and crustal-scale faults.

456   Below the Miocene sedimentary filling, Andalucia-A1 well reveals ~190m of phyllitic and quartzitic meta-sediments

457   (2.4 to 4 s TWT below the Alboran basin, **Figs. 13** and **14**) topped by Langhian to Tortonian marls (top at ~1.6 to 3.4

458   s TWT below the Alboran basin) interbedded with Tortonian-Messinian tuffs and basaltic lavas. These units have

459   been correlated in the magmatic arc crust of EAB after Gomez de la Peña et al. (2020b). The older deposits (Unit V)

460   Langhian-Serravallian in age, consist of clays and marls with intercalated sands and volcano-clastic deposits. The

461   seismic facies of this Unit V is made of moderate amplitude and low frequency discontinuous reflections packages

462   (Figure 18), and is only present in the Northern Alboran Basin. They are correlated with volcanic series in the EAB

463   (vY3) (Gomez de la Peña et al., 2020b). They pass upward into Serravallian sand-silty clay turbidite (Unit IV) possibly

464   correlated with volcanic series in EAB (vY2 after Gomez de la Peña et al., 2020b). This unit exhibiting low to moderate

465   amplitude, moderate frequency drawing continuous sheeted to disrupted reflectors, is unconformably overlying Unit

466   V and locally onlaps onto the basement. Thickness of Unit IV remains rather thin in the North and East Alboran Basin.

467   It can't be properly identified in the South Balearic Basin, east of the Maimonides volcanic ridge (**Fig. 15**). The Unit

468   III dated from late Serravallian to late Tortonian is represented by sandstones interbedded with volcano-clastic levels

469   whih correlates in EAB with volanics vY1 unit. Unit III contains internal reflections characterized by low to moderate

470   amplitude, moderate frequency continuous sheeted reflectors. Its thickness remains relatively constant from the NAB

471   to the EAB, and is identified beneath the Messinian Unit II in the South Balearic Basin. Unit II corresponds to the

472   Messinian evaporite, carbonate, volcanic, and volcaniclastic deposits interbedded with fine-grained sediments and is

473   equivalent to unit III of (Peña et al., 2020b) in EAB. Seismic facies of Unit II is marked in the Alboran domain by

474   lower amplitudes and lower frequency reflectors. In ESCI-Alb2b line, Unit II increases drastically east of the

475   Maimonides ridge, which delimits the western boundary of the salt deposits in the Western Mediterranean basin during

476   the Messinian Salinity Crisis (Haq et al., 2020). Unit II is topped by Unit I made of Pliocene to Quaternary clays and

477   sanstones, which are correlated with units II and I in EAB (Gomez de la Peña et al., 2020b). Unit I is marked by thinly
478   bedded, mostly parallel, high-frequency and low amplitudes reflectors (**Fig. 18**). Its thickness fluctuates in response
479   to sedimentary processes (Juan et al., 2016).
480   Along line MSB08 (**Fig. 14**) the Langhian-Serravallian (Unit V) is maximum 1600 m-thick (using a P-wave velocity
481   of 3.2 km/s calculated within Andalucia-A1 well. In EAB, south of Carboneras Fault Zone, the total thickness of Unit
482   V is only ~300 m on MSB07 (**Fig. 13**) and is absent in ESCI-Alb2b (**Fig. 15**). The Serravallian-Tortonian (Unit IV-
483   III) interval shows only very limited sediment accumulation (~300 m) except near the NW-SE oriented normal faults
484   where growth geometries are visible. These normal faults are sealed by the Tortonian-Messinian deposits, indicating
485   a syn-sedimentary faulting during the middle Miocene (**Fig. 13**). With respect to offshore observations this
486   sedimentary infill is more continuous and is also much thinner conpared to TB and HOB where they are represented
487   by thick conglomerates and marls/turbidites (> 1km) (**Fig. 7**), and they are eroded or not deposited along the axes of
488   the metamorphic domes. The Messinian deposits (Unit II) are ~150-350 m-thick north of CF (MSB07-08 ; **Figs. 13,**
489   **14**) and increase to about 1200 m eastward in the eastern EAB (ESCI-Alb2b ; **Fig. 15**), and in Algero-Balearic basin
490   (Gomez de la Peña et al., 2020b). The top Messinian reflector is topped by thick horizontal sedimentary strata, with a
491   maximum thickness of 1.2 s TWT (~2.4 km assuming a velocity of 2 km/s) on line MSB07, suggesting an important
492   channel system during the Pliocene.
493   The Pliocene-to-Quaternary series are poorly deformed except in the vicinity of CF and near the Alboran Ridge where
494   this is associated with south-dipping reverse fault (**Fig. 13**). This late and still active compressional tectonics is
495   revealed by the overthrusting of the SAB over the south margin of the EAB e.g. (Martínez-García et al., 2011).
496
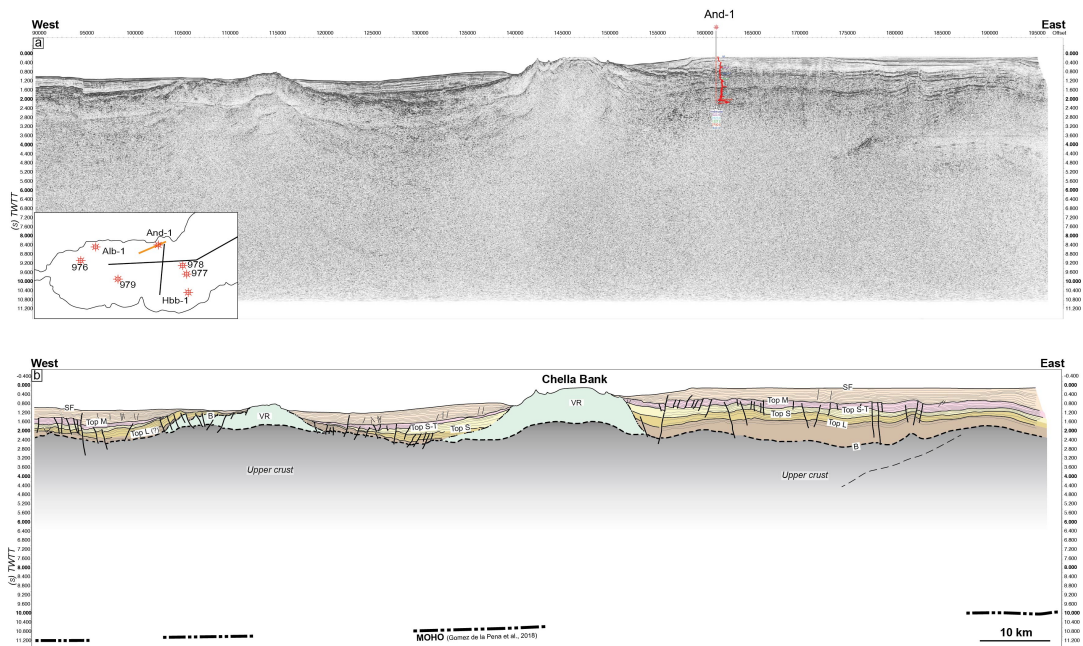
497

498   **Figure 14** : Seismic reflection line MSB08 (see location on **Fig. 1**). See Figure 13 for abbreviations. See also Figure
499   S3 showing a zoom on the main seismic facies recognized in Andalucia-A1 well.
500

501
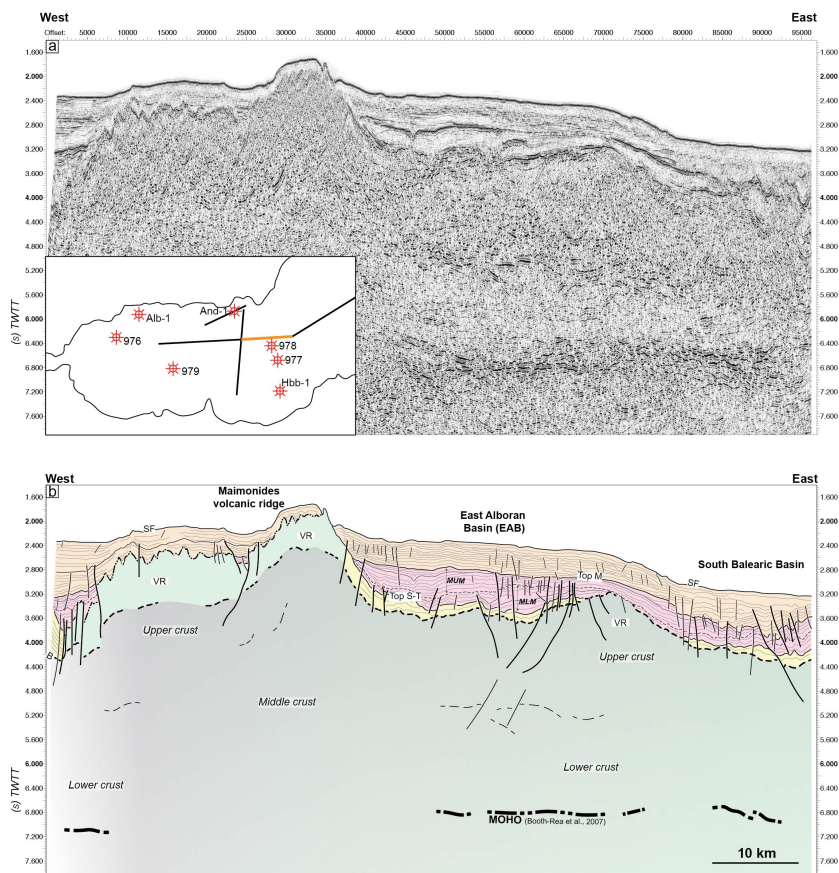
502   **Figure 15**. (**a, b**) Seismic reflection line ESCI-Alb2b and intepretation (see Figure 1 for location). Seismic units are
503   correlated with those defined by Booth-Rea et al. (2007). See Figure 13 for abbreviations.
504

505

506
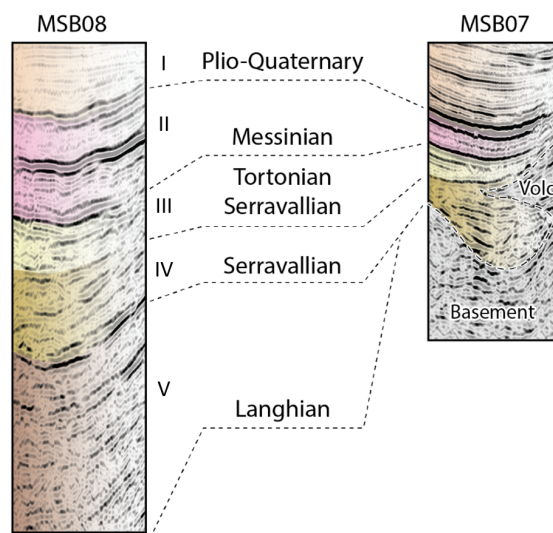
Figure 16 : Seismic facies of units I to V seen through seismic lines MSB08 close to the shoreline and the line
MSB07, located deeper in the East Alboran Basin.

5.2 N-S crustal cross-section of the Alboran margin accounting for strike-slip faulting

Based on subsurface constraints and field data, we have built a crustal cross-section across the rifted margin from the
Sierra de las Estancias and Huercal-Overa basin (HOB), which represents the proximal margin, to the center of the
Alboran margin (**Fig. 17**). The proximal margin is defined by a 30-35 km-thick crust. It preserves part of the thickness
acquired during former orogenic phase that has been little involved in crustal thinning. The onset of crustal thinning
to the south is recorded by the formation of strongly subsident and asymmetric basins of the HOB and TB, shaping
the upper neck domain. This domain is characterized by orthogonal and oblique extension during the Tortonian
accommodated by normal and strike-slip faulting. This boundary also corresponds to the position of the major STEP
fault documented by seismology. From the Sierra de los Filabres to the south, the crustal thickness reduces to 25 km
in the Tabernas basin along the Alpujarras strike-slip corridor and below the Sierra Alhamilla. The Nijar basin depicts
the transition towards offshore distal domains with a crustal thickness of 20 km. The Tortonian and Messinian marine
sediments are also thicker and a number of volcanic bodies accompany crustal thinning. Crustal thinning appears
localized along the Carboneras Fault (CF), which juxtaposed crust with different crustal thickness (**Fig. 19**). South of
CF, the crust thickness reduces below 20 km and shows increasing magmatic additions making the magmatic arc crust
of the EAB (Gomez de la Peña et al., 2018 ; 2020). Interestingly, normal faulting in the EAB is sealed by middle-
upper Tortonian deposits. Crustal deformation then shifted to the north in the CF and EBSZ strike-slip fault zones and
to the south along the Alboran Ridge where reverse faulting occurred.
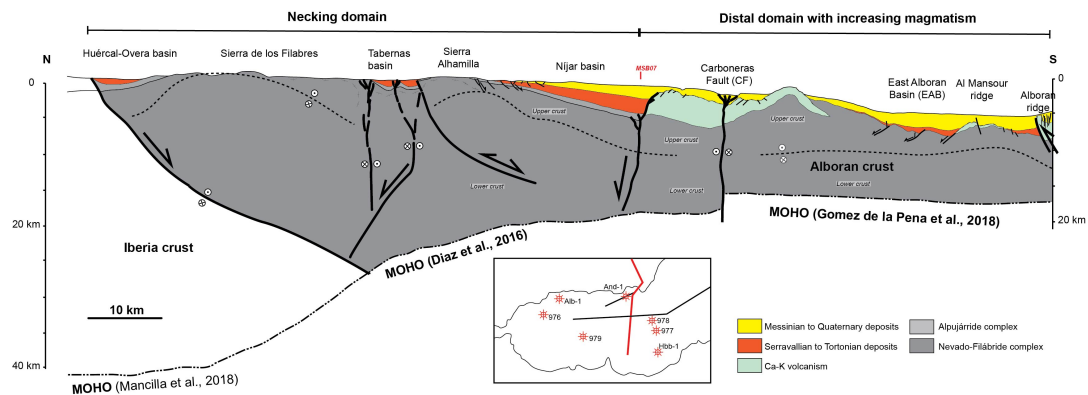
Figure 17. Crustal-scale cross section of the Alboran margin in the eastern Betics interpreted based on onshore and offshore contraints presented in the text. Note that in the necking domain the extension of faults downwards to Moho depths is not imaged on the seismics and therefore largely inspired by inferences from 3D numerical models (see Fig. 3).

7. Implications

The question of whether the Miocene tectonic evolution of the Betics reflects crustal thinning associated with oblique back-arc rifting as suggested from present-day strain patterns is unclear in the literature. Back-arc extension, recent tectonic inversion and STEP faulting are generally considered to result from separated processes. We found based on a comparison between numerical models and analyses of basin evolution, fault kinematics and structure of the margin in the eastern Betics compelling evidences that crustal thinning occurred under oblique extension and was not restricted to the post-Tortonian evolution. Rather, oblique rifting possibly operated since at least the middle Miocene, as the slab retreat started in the Alboran basin and is therefore kinematically associated with STEP faulting.

One of the most striking tectonic feature of the Alboran margin (**Fig. 17**) is the abrupt N-S crustal thinning, from 35-30 km to 25-20 km, oblique to the direction of slab retreat. The history of sediment infill and rates of subsidence in intramontane basins (**Figs. 6 and 7**) combined with the analyses of fault slip data, confirm that brittle extension oriented from N20°E to EW occurred during an interval spanning from the Serravallian-early Tortonian to the late Tortonian (14-8 Ma). This extension is found associated with both normal and strike-slip regimes. In more details, these data suggest that N20°E extension is more represented in HOB, while the ENE-WSW to EW extension is found related with the evolution of the Almanzora corridor, Alpujarras corridor and Tarbenas basin flanking the metamorphic domes (**Table S1**). There are additional evidence that EW-directed dextral strike-slip faulting did occur during the Tortonian to the South and West of the HOB and represents this main phase of basin subsidence. These large-scale faults are later cut by Tortonian NW-SE faults that argue for more recent EW extension. Therefore, we infer that the domain south of the HOB, which also corresponds to a thinnest crust, has experienced transtensional deformation and EW extension.

554
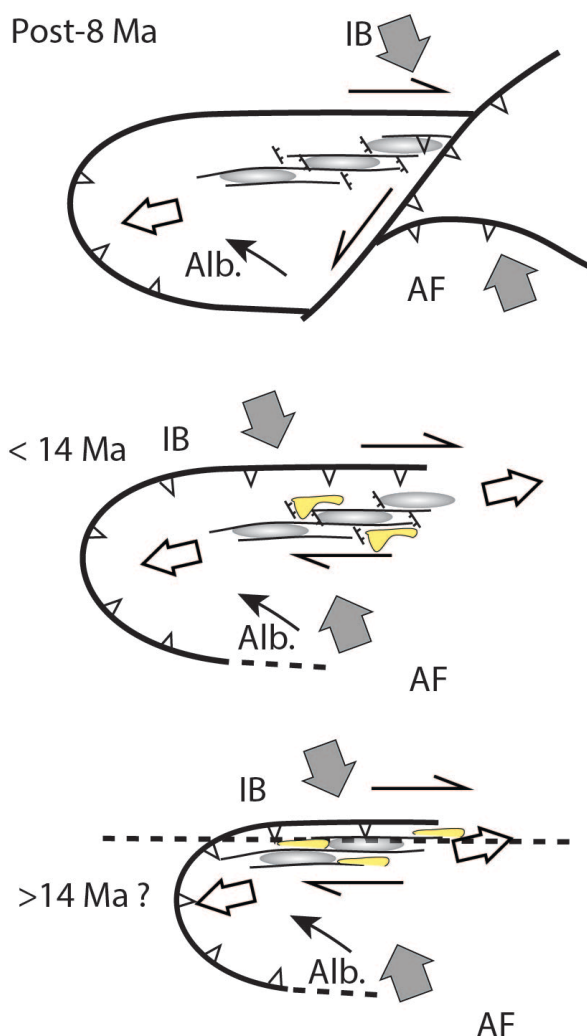
Figure 18: Tectonic model of the evolution of the northern margin of the Alboran Rift. Large grey and white double arrows depict shortening, which is parallel to the AF/IB convergence, and the highly oblique extension, respectively. The thin black arrows is showing the motion of Alboran relative to Iberia (IB) taken from Figure 4. Half arrows depicts the distributed strike-slip faulting in the Betics. NW-SE directed normal fault and strike-slip basins (yellow) are consistent with the oblique extension. Grey-shaded ellipses represent the metamorphic domes.

Several key specific tectonic features found in the eastern Betics are predicted by 3D models of oblique extension (**Figure 3**). Those include the E-W trending faults that are prevalent on the upper neck domain (i.e. Sierra de las Estancias and HOB), and E-W strike-slip faults (Almanzora and Alpujarras corridor) and NW-SE normal faults that are found associated with more distal domains where crustal thinning is the highest. Brittle E-W-directed stretching and dextral transcurrent deformation started in the Langhian-Serravallian (14-13 Ma). Tectonic inversion seems, in contrast, to have been increasingly more important when approaching the Carboneras and Palomeras strike-slip faults in the East since the late Tortonian.

568   According to temporal constraints, ductile thinning may have occurred between 23 to 16 Ma prior to brittle faulting
569   at 14-13 Ma (**Figure 18**). The late/post-Tortonian times marks a change in the tectonic evolution of the region (Jolivet
570   et al., 2021a; Mouthereau et al., 2021; Rat et al., 2022) as the mantle slab eventually detached and is responsible for
571   Ca-K magmatism at 11-7 Ma (Duggen et al., 2008, 2004), compression and tightening of the metamorphic domes
572   associated with the formation of the the EBSZ.

573   The strike-slip deformation model has the advantage to explain N-S crustal thinning in the Betics while back-arc
574   extension is oriented E-W, in a continuum of deformation from the Miocene to the present. In this model, ductile
575   stretching and ductile detachment associated with the development of the domes are the expression of oblique E-W
576   extension. This provides a coherent scheme linking the formation of EW-directed basins in the brittle field associated
577   with strike-slip faulting, and NW-SE/NNW-SSE sedimentary basins (Guadix, Baza, Alhabia) formed in transtension
578   during the Tortonian. As such, the oblique extension, which is closely associated with STEP faulting required by slab
579   retreat, is overall a characteristic feature of the regional NW-SE/NNW-SSE convergence since at least the Miocene.
580   Only recently, around 8 Ma, as the slab detached, shortening started to prevail in the vicinity of the EBSZ (**Figure
581   18**). As convergence was under way during oblique back-arc extension, high-pressure metamorphism and subduction
582   possibly occurred during the mid-Miocene as argued in eastern Betics (Platt et al., 2013). Moreover, the case of
583   exhumation of high-pressure rocks in oblique convergence setting associated with near-parallel orogeni extension is
584   documented in other active orogen like Taiwan (Conand et al., 2020).

585   This highly oblique northern Alboran margin differs from typical transform fault margin such as those associated with
586   the Altantic ocean because it accommodates variations in intra-plate extensional movements, triggered by slab roll-
587   back not variations in spreading rates. Strike-slip faults may have originated as low-angle normal which were later
588   reactivated as thrusts during margin inversion. Similar observations, including metamorphism, strike-slip faulting,
589   high geothermal gradients and volcanism has been made in Seram, north of the Banda Arc, which represents an other
590   example of extremely thinned crust formed perpendicular to the direction of the slab retreat (Pownall et al., 2013).
591   Such a narrow rifted margin associated with lithospheric STEP fault defines a class of oblique (and transform) margin
592   that is expected to be hardly preserved in the geological record due the transient nature of retreating subduction
593   systems.

594

595   **Data availability**.This study is based on data compilation. Data used in this study can be found in the appropriate
596   references. Paleostress tensors obtained by the inversion of fault slip data are available online in the Supplement.

597

598   **Supplement**.The supplement related to this article is available on-line at:

599

600   **Competing interests**.The authors declare that they have no conflictof interest.

601   **Authors contribution**

602   ML and FM, conceptualize, prepared figures and tables, compiled and interpreted field structural data and wrote the
603   paper. DC provided and interpreted the seismic lines, reviewed the text and contributed to the writing. AJ carefully

604   exmined the implementation of his numerical results and reviewed the text. EM, SC and VM, supervised and

605   coordinate the different project tasks and reviewed the text.

606   **Acknowledgments**

607   The stereogram results were obtained using Win-Tensor, a software developed by Dr. Damien Delvaux, Royal

608   Museum for Central Africa, Tervuren, Belgium (Delvaux and Sperner, 2003). The processed seismic data were

609   interpreted using Kingdom IHS Suite© software. This research benefited from discussions and support of OROGEN

610   project, an academic-industry research consortium between TOTAL, CNRS and BRGM.

611

612

References

Angrand, P., Mouthereau, F., 2021. Evolution of the Alpine orogenic belts in the Western Mediterranean region as resolved by the kinematics of the Europe-Africa diffuse plate boundary. Bsgf - Earth Sci Bulletin. https://doi.org/10.1051/bsgf/2021031

Argus, D.F., Gordon, R.G., DeMets, C., 2011. Geologically current motion of 56 plates relative to the no-net-rotation reference frame. Geochemistry, Geophysics, Geosystems 12. https://doi.org/10.1029/2011gc003751

Augier, R., 2004. Evolution tardi-orogénique des Cordillères Betiques (Espagne) : apports d'une étude integrée 1 vol., [II]-400 p.

Augier, R, Agard, P., Monié, P., Jolivet, L., Robin, C., Booth-Rea, G., 2005. Exhumation, doming and slab retreat in the Betic Cordillera (SE Spain): in situ40Ar/39Ar ages and P–T–d–t paths for the Nevado-Filabride complex. Journal of Metamorphic Geology 23, 357–381. https://doi.org/10.1111/j.1525-1314.2005.00581.x

Augier, Romain, Booth-Rea, G., Agard, P., Martínez-Martínez, J.M., Jolivet, L., Azañón, J.M., 2005a. Exhumation constraints for the lower Nevado-Filabride Complex (Betic Cordillera, SE Spain): a Raman thermometry and Tweequ multiequilibrium thermobarometry approach. Bulletin de la Societe Geologique de France 176, 403–416. https://doi.org/10.2113/176.5.403

Augier, R., Jolivet, L., couto, D.D., Negro, F., 2013. From ductile to brittle, late- to post-orogenic evolution of the Betic Cordillera: Structural insights from the northeastern Internal zones. Bulletin De La Société Géologique De France 184, 405–425. https://doi.org/10.2113/gssgfbull.184.4-5.405

Augier, Romain, Jolivet, L., Robin, C., 2005b. Late Orogenic doming in the eastern Betic Cordilleras: Final exhumation of the Nevado-Filabride complex and its relation to basin genesis. Tectonics 24, n/a-n/a. https://doi.org/10.1029/2004tc001687

Badji, R., Charvis, P., Bracene, R., Galve, A., Badsi, M., Ribodetti, A., Benaissa, Z., Klingelhoefer, F., Medaouri, M., Beslier, M.-O., 2014. Geophysical evidence for a transform margin offshore Western Algeria: a witness of a subduction-transform edge propagator? Geophys J Int 200, 1029–1045. https://doi.org/10.1093/gji/ggu454

Bessière, E., Jolivet, L., Augier, R., Scaillet, S., Précigout, J., Azañón, J.-M., Crespo-Blanc, A., Masini, E., Couto, D.D., 2021. Lateral variations of pressure-temperature evolution in non-cylindrical orogens and 3-D subduction dynamics: the Betic-Rif Cordillera example. Bsgf - Earth Sci Bulletin. https://doi.org/10.1051/bsgf/2021007

Bezada, M.J., Humphreys, E.D., Toomey, D.R., Harnafi, M., Dávila, J.M., Gallart, J., 2013. Evidence for slab rollback in westernmost Mediterranean from improved upper mantle imaging. Earth and Planetary Science Letters 368, 51–60. https://doi.org/10.1016/j.epsl.2013.02.024

Booth-Rea, G., Martínez-Martínez, J.M., Giaconia, F., 2015. Continental subduction, intracrustal shortening, and coeval upper-crustal extension: P-T evolution of subducted south Iberian paleomargin metapelites (Betics, SE Spain). Tectonophysics 663, 122–139. https://doi.org/10.1016/j.tecto.2015.08.036

Booth-Rea, G., Ranero, C.R., Grevemeyer, I., 2018. The Alboran volcanic-arc modulated the Messinian faunal exchange and salinity crisis. Scientific reports 8, 13015. https://doi.org/10.1038/s41598-018-31307-7

Booth-Rea, G., Ranero, C.R., Martinez-Martinez, J.M., Grevemeyer, I., 2007. Crustal types and Tertiary tectonic evolution of the Alborán sea, western Mediterranean. Geochemistry, Geophysics, Geosystems 8, n/a-n/a. https://doi.org/10.1029/2007gc001639

Borque, M.J., Alzola, A.S., Martin-Rojas, I., Alfaro, P., Molina, S., Cintas, S.R., Caderot, G.R., Lacy, C., Avilés, M., Olmo, A.H., Tortosa, F.J.G., Estévez, A., Gil, A.J., 2019. How Much Nubia-Eurasia Convergence Is Accommodated by the NE End of the Eastern Betic Shear Zone (SE Spain)? Constraints From GPS Velocities. Tectonics 38, 271–1839. https://doi.org/10.1029/2018tc004970

Braga, J.C., Martín, J.M., Quesada, C., 2003. Patterns and average rates of late Neogene–Recent uplift of the Betic Cordillera, SE Spain. Geomorphology 50, 3–26. https://doi.org/10.1016/s0169-555x(02)00205-2

Carbonell, R., Sallares, V., Pous, J., Dañobeitia, J.J., Queralt, P., Ledo, J.J., Dueñas, V.G., 1998. A multidisciplinary geophysical study in the Betic chain (southern Iberia Peninsula). Tectonophysics 288, 137–152. https://doi.org/10.1016/s0040-1951(97)00289-8

Clark, S.J.P., Dempster, T.J., 2009. The record of tectonic denudation and erosion in an emerging orogen: an apatite fission-track study of the Sierra Nevada, southern Spain. Journal of the Geological Society 166, 87–100. https://doi.org/10.1144/0016-76492008-041

Comas, M. C., J. J. Dañobeitia, J. Alvarez-Maron, and J. I. Soto (1995), Crustal reflections and structure in the Alboran Basin. Preliminary results of the ESCI-Alboran survey, Rev. Soc. Geol. Esp., 8(4), 529 – 542.

Comas, M.C., García-Dueñas, V., Jurado, M.J., 1992. Neogene tectonic evolution of the Alboran Sea from MCS data. Geo-mar Lett 12, 157–164. https://doi.org/10.1007/bf02084927

667 Comas, M., and MARSIBAL 1-06 Scientific Party (2007). Preliminary results of Marsibal 1-06 cruise in the
668   Alboran and western Algero-Balearic basins. Geophys. Res. Abst., 9, 10871.
669 Conand, C., Mouthereau, F., Ganne, J., Lin, A.T., Lahfid, A., Daudet, M., Mesalles, L., Giletycz, S., Bonzani, M.,
670   2020. Strain Partitioning and Exhumation in Oblique Taiwan Collision: Role of Rift Architecture and Plate
671   Kinematics. Tectonics 39, e2019TC005798. https://doi.org/10.1029/2019tc005798
672 Couto, D.D., Gumiaux, C., Augier, R., Lebret, N., Folcher, N., Jouannic, G., Jolivet, L., Suc, J., Gorini, C., 2014.
673   Tectonic inversion of an asymmetric graben: Insights from a combined field and gravity survey in the Sorbas
674   basin. Tectonics 33, 1360–1385. https://doi.org/10.1002/2013tc003458
675 Crespo-Blanc, A., Comas, M., Balanyá, J.C., 2016. Clues for a Tortonian reconstruction of the Gibraltar Arc:
676   Structural pattern, deformation diachronism and block rotations. Tectonophysics 683, 308–324.
677   https://doi.org/10.1016/j.tecto.2016.05.045
678 d'Acremont, E., Lafosse, M., Rabaute, A., Teurquety, G., Couto, D.D., Ercilla, G., Juan, C., Lépinay, B.M.,
679   Lafuerza, S., Galindo-Zaldivar, J., Estrada, F., Vazquez, J.T., Leroy, S., Poort, J., Ammar, A., Gorini, C., 2020.
680   Polyphase Tectonic Evolution of Fore-Arc Basin Related to STEP Fault as Revealed by Seismic Reflection Data
681   From the Alboran Sea (W-Mediterranean). Tectonics 39. https://doi.org/10.1029/2019tc005885
682 Dalziel, I.W.D., Lawver, L.A., Norton, I.O., Gahagan, L.M., 2013. The Scotia Arc: Genesis, Evolution, Global
683   Significance. Annu Rev Earth Pl Sc 41, 767–793. https://doi.org/10.1146/annurev-earth-050212-124155
684 Daudet, M., Mouthereau, F., Brichau, S., Crespo-Blanc, A., Gautheron, C., Angrand, P., 2020. Tectono-
685   Stratigraphic and Thermal Evolution of the Western Betic Flysch: Implications for the Geodynamics of South
686   Iberian Margin and Alboran Domain. Tectonics 39. https://doi.org/10.1029/2020tc006093
687 Dewey, J.F., 1988. Extensional collapse of orogens. Tectonics 7, 1123–1139.
688   https://doi.org/10.1029/tc007i006p01123
689 Dewey, J.F., Helman, M.L., Knott, S.D., Turco, E., Hutton, D.H.W., 1989. Kinematics of the western
690   Mediterranean. Geological Society, London, Special Publications 45, 265–283.
691   https://doi.org/10.1144/gsl.sp.1989.045.01.15
692 Diaz, J., Gallart, J., Carbonell, R., 2016. Moho topography beneath the Iberian-Western Mediterranean region
693   mapped from controlled-source and natural seismicity surveys. Tectonophysics 692, 74–85.
694   https://doi.org/10.1016/j.tecto.2016.08.023
695 Duggen, S., Hoernle, K., Bogaard, P. van den, Harris, C., 2004. Magmatic evolution of the Alboran region: The role
696   of subduction in forming the western Mediterranean and causing the Messinian Salinity Crisis. Earth Planet Sc
697   Lett 218, 91–108. https://doi.org/10.1016/s0012-821x(03)00632-0
698 Duggen, S., Hoernle, K., Klügel, A., Geldmacher, J., Thirlwall, M., Hauff, F., Lowry, D., Oates, N., 2008.
699   Geochemical zonation of the Miocene Alborán Basin volcanism (westernmost Mediterranean): geodynamic
700   implications. Contrib Mineral Petr 156, 577. https://doi.org/10.1007/s00410-008-0302-4
701 Echeverria, A., Khazaradze, G., Asensio, E., Gárate, J., Dávila, J.M., Suriñach, E., 2013. Crustal deformation in
702   eastern Betics from CuaTeNeo GPS network. Tectonophysics 608, 600–612.
703   https://doi.org/10.1016/j.tecto.2013.08.020
704 Faccenna, C., Becker, T.W., Auer, L., Billi, A., Boschi, L., Brun, J.P., Capitanio, F.A., Funiciello, F., Horvàth, F.,
705   Jolivet, L., Piromallo, C., Royden, L., Rossetti, F., Serpelloni, E., 2014. Mantle dynamics in the Mediterranean.
706   Rev Geophys 52, 283–332. https://doi.org/10.1002/2013rg000444
707 Fortuin, A.R., Krijgsman, W., 2003. The Messinian of the Nijar Basin (SE Spain): sedimentation, depositional
708   environments and paleogeographic evolution. Sediment Geol 160, 213–242. https://doi.org/10.1016/s0037-
709   0738(02)00377-9
710 Fossen, H., Teyssier, C., Whitney, D.L., 2013. Transtensional folding. Journal of structural geology 56, 89–102.
711   https://doi.org/http://dx.doi.org/10.1016/j.jsg.2013.09.004
712 Fossen, H., Tikoff, B., 1998. Extended models of transpression and transtension, and application to tectonic settings.
713   Geological Society, London, Special Publications 135, 15–33. https://doi.org/10.1144/gsl.sp.1998.135.01.02
714 Frasca, G., Gueydan, F., Brun, J.-P., Monié, P., 2016. Deformation mechanisms in a continental rift up to mantle
715   exhumation. Field evidence from the western Betics, Spain. Mar Petrol Geol 76, 310–328.
716   https://doi.org/10.1016/j.marpetgeo.2016.04.020
717 Galindo-Zaldivar, J., Gonzalez-Lodeiro, F., Jabaloy, A., 2015. Progressive extensional shear structures in a
718   detachment contact in the Western Sierra Nevada (Betic Cordilleras, Spain). Geodin Acta 3, 73–85.
719   https://doi.org/10.1080/09853111.1989.11105175
720 Galindo-Zaldivar, J., Gil, A.J., Borque, M.J., González-Lodeiro, F., Jabaloy, A., Marin-Lechado, C., Ruano, P.,
721   Galdeano, C.S. de, 2003. Active faulting in the internal zones of the central Betic Cordilleras (SE, Spain). J
722   Geodyn 36, 239–250. https://doi.org/10.1016/s0264-3707(03)00049-8

723   Gallais, F., Graindorge, D., Gutscher, M.-A., Klaeschen, D., 2013. Propagation of a lithospheric tear fault (STEP)
724   through the western boundary of the Calabrian accretionary wedge offshore eastern Sicily (Southern Italy).
725   Tectonophysics 602, 141–152. https://doi.org/10.1016/j.tecto.2012.12.026
726   García-Dueñas, V., Banda, E., Torné, M., Córdoba, D., Group, E.-B.W., 1994. A deep seismic reflection survey
727   across the Betic Chain (southern Spain): first results. Tectonophysics 232, 77–89. https://doi.org/10.1016/0040-
728   1951(94)90077-9
729   Giaconia, F., Booth-Rea, G., Martínez-Martínez, J.M., Azañón, J.M., Pérez-Romero, J., Villegas, I., 2013. Mountain
730   front migration and drainage captures related to fault segment linkage and growth: The Polopos transpressive
731   fault zone (southeastern Betics, SE Spain). J Struct Geol 46, 76–91. https://doi.org/10.1016/j.jsg.2012.10.005
732   Gomez-Pugnaire, M.T., Fernandez-Soler, J.M., 1987. High-pressure metamorphism in metabasites from the Betic
733   Cordilleras (S.E. Spain) and its evolution during the Alpine orogeny. Contrib Mineral Petr 95, 231–244.
734   https://doi.org/10.1007/bf00381273
735   Govers, R., Wortel, M.J.R., 2005. Lithosphere tearing at STEP faults: response to edges of subduction zones. Earth
736   Planet Sc Lett 236, 505–523. https://doi.org/10.1016/j.epsl.2005.03.022
737   Haq, B., Gorini, C., Baur, J., Moneron, J., & Rubino, J.-L. (2020). Deep Mediterranean's Messinian evaporite giant:
738   How much salt? Global and Planetary Change, 184, 103052.
739   doi:https://doi.org/10.1016/j.gloplacha.2019.103052
740   Haughton, P.D.W., 2000. Evolving turbidite systems on a deforming basin floor, Tabernas, SE Spain.
741   Sedimentology 47, 497–518. https://doi.org/10.1046/j.1365-3091.2000.00293.x
742   Haughton, P.D.W., 1994. Deposits of deflected and ponded turbidity currents, Sorbas Basin, Southeast Spain. J
743   Sediment Res 64, 233–246. https://doi.org/10.1306/d4267d6b-2b26-11d7-8648000102c1865d
744   Heit, B., Mancilla, F. de L., Yuan, X., Morales, J., Stich, D., Martín, R., Molina-Aguilera, A., 2017. Tearing of the
745   mantle lithosphere along the intermediate-depth seismicity zone beneath the Gibraltar Arc: The onset of
746   lithospheric delamination. Geophys Res Lett 44, 4027–4035. https://doi.org/10.1002/2017gl073358
747   Hinsbergen, D.J.J., Vissers, R.L.M., Spakman, W., 2014. Origin and consequences of western Mediterranean
748   subduction, rollback, and slab segmentation. Tectonics 33, 393–419. https://doi.org/10.1002/2013tc003349
749   Hodgson, D.M., Haughton, P.D.W., 2004. Impact of syndepositional faulting on gravity current behaviour and deep-
750   water stratigraphy: Tabernas-Sorbas Basin, SE Spain. Geological Soc Lond Special Publ 222, 135–158.
751   https://doi.org/10.1144/gsl.sp.2004.222.01.08
752   Janowski, M., Loget, N., Gautheron, C., Barbarand, J., BELLAHSEN, N., Driessche, J.V. den, Babault, J., Meyer,
753   B., 2017. Neogene exhumation and relief evolution in the eastern Betics (SE Spain): Insights from the Sierra de
754   Gador. Terra Nova 29, 91–97. https://doi.org/10.1111/ter.12252
755   Johnson, C., Harbury, N., Hurford, A.J., 1997. The role of extension in the Miocene denudation of the Nevado-
756   Filábride Complex, Betic Cordillera (SE Spain). Tectonics 16, 189–204. https://doi.org/10.1029/96tc03289
757   Jolivet, L., Baudin, T., Calassou, S., Chevrot, S., Ford, M., Issautier, B., Lasseur, E., Masini, E., Manatschal, G.,
758   Mouthereau, F., Thinon, I., Vidal, O., 2021a. Geodynamic evolution of a wide plate boundary in the Western
759   Mediterranean, near-field versus far-field interactions. Bsgf - Earth Sci Bulletin 192, 48.
760   https://doi.org/10.1051/bsgf/2021043
761   Jolivet, L., Faccenna, C., 2000. Mediterranean extension and the Africa-Eurasia collision. Tectonics 19, 1095–1106.
762   https://doi.org/10.1029/2000tc900018
763   Jolivet, L., Menant, A., Roche, V., Pourhiet, L.L., Maillard, A., Augier, R., Couto, D.D., Gorini, C., Thinon, I.,
764   Canva, A., 2021b. Transfer zones in Mediterranean back-arc regions and tear faults. Bsgf - Earth Sci Bulletin
765   192, 11. https://doi.org/10.1051/bsgf/2021006
766   Jourdon, A., Kergaravat, C., Duclaux, G., Huguen, C., 2021. Looking beyond kinematics: 3D thermo-mechanical
767   modelling reveals the dynamics of transform margins. Solid Earth 12, 1211–1232. https://doi.org/10.5194/se-12-
768   1211-2021
769   Juan, C., Ercilla, G., Javier Hernández-Molina, F., Estrada, F., Alonso, B., Casas, D., . . . Ammar, A. (2016).
770   Seismic evidence of current-controlled sedimentation in the Alboran Sea during the Pliocene and Quaternary:
771   Palaeoceanographic implications. Marine Geology, 378, 292-311.
772   doi:https://doi.org/10.1016/j.margeo.2016.01.006
773   Jurado, M.J., Comas, M.C., 1992. Well log interpretation and seismic character of the cenozoic sequence in the
774   northern Alboran Sea. Geo-Marine Letters 12, 129–136.
775   Kleverlaan, K., 1989. Neogene history of the Tabernas basin (SE Spain) and its Tortonian submarine fan
776   development. Geologie en Mijnbouw 421–432.
777   Kleverlaan, K., 1989. Three distinctive feeder-lobe systems within one time slice of the Tortonian Tabernas fan, SE
778   Spain. Sedimentology 36, 25–45. https://doi.org/10.1111/j.1365-3091.1989.tb00818.x

779 Kleverlaan, K., 1987. Gordo megabed: a possible seismite in a tortonian submarine fan, tabernas basin, province
780   almeria, southeast spain. Sediment Geol 51, 165–180. https://doi.org/10.1016/0037-0738(87)90047-9
781 Koulali, A., Ouazar, D., Tahayt, A., King, R.W., Vernant, P., Reilinger, R.E., McClusky, S., Mourabit, T., Davila,
782   J.M., Amraoui, N., 2011. New GPS constraints on active deformation along the Africa–Iberia plate boundary.
783   Earth Planet Sc Lett 308, 211–217. https://doi.org/10.1016/j.epsl.2011.05.048
784 Larouzière, F.D.D., Bolze, J., Bordet, P., Hernandez, J., Montenat, C., d'Estevou, P.O., 1988. The Betic segment of
785   the lithospheric Trans-Alboran shear zone during the Late Miocene. Tectonophysics 152, 41–52.
786   https://doi.org/10.1016/0040-1951(88)90028-5
787 Lonergan, L., White, N., 1997. Origin of the Betic-Rif mountain belt. Tectonics 16, 504–522.
788   https://doi.org/10.1029/96tc03937
789 Mancilla, F. de L., Booth-Rea, G., Stich, D., Pérez-Peña, J.V., Morales, J., Azañón, J.M., Martin, R., Giaconia, F.,
790   2015a. Slab rupture and delamination under the Betics and Rif constrained from receiver functions.
791   Tectonophysics. https://doi.org/10.1016/j.tecto.2015.06.028
792 Mancilla, F. de L., Heit, B., Morales, J., Yuan, X., Stich, D., Molina-Aguilera, A., Azañón, J.M., Martín, R., 2018.
793   A STEP fault in Central Betics, associated with lateral lithospheric tearing at the northern edge of the Gibraltar
794   arc subduction system. Earth Planet Sc Lett 486, 32–40. https://doi.org/10.1016/j.epsl.2018.01.008
795 Mancilla, F. de L., Stich, D., Morales, J., Martin, R., Diaz, J., Pazos, A., Córdoba, D., Pulgar, J.A., Ibarra, P.,
796   Harnafi, M., Gonzalez-Lodeiro, F., 2015b. Crustal thickness and images of the lithospheric discontinuities in the
797   Gibraltar arc and surrounding areas. Geophysical Journal International 203, 1804–1820.
798   https://doi.org/10.1093/gji/ggv390
799 Martin, J.M., Braga, J.C., Rivas, P., 1989. Coral successions in Upper Tortonian reefs in SE Spain. Lethaia 22, 271–
800   286. https://doi.org/10.1111/j.1502-3931.1989.tb01342.x
801 Martín, JoséM., Braga, J.C., 1994. Messinian events in the Sorbas Basin in southeastern Spain and their implications
802   in the recent history of the Mediterranean. Sediment Geol 90, 257–268. https://doi.org/10.1016/0037-
803   0738(94)90042-6
804 Martínez-García, P., Comas, M., Lonergan, L., Watts, A.B., 2017. From Extension to Shortening: Tectonic
805   Inversion Distributed in Time and Space in the Alboran Sea, Western Mediterranean. Tectonics 36, 2777–2805.
806   https://doi.org/10.1002/2017tc004489
807 Martínez-García, P., Soto, J.I., Comas, M., 2011. Recent structures in the Alboran Ridge and Yusuf fault zones
808   based on swath bathymetry and sub-bottom profiling: evidence of active tectonics. Geo-mar Lett 31, 19–36.
809   https://doi.org/10.1007/s00367-010-0212-0
810 Martínez-Martínez, J.M., Azañón, J.M., 1997. Mode of extensional tectonics in the southeastern Betics (SE Spain):
811   Implications for the tectonic evolution of the peri-Alborán orogenic system. Tectonics 16, 205–225.
812   https://doi.org/10.1029/97tc00157
813 Martínez-Martínez, J.M., Booth-Rea, G., Azañón, J.M., Torcal, F., 2006. Active transfer fault zone linking a
814   segmented extensional system (Betics, southern Spain): Insight into heterogeneous extension driven by edge
815   delamination. Tectonophysics 422, 159–173. https://doi.org/10.1016/j.tecto.2006.06.001
816 Martínez-Martínez, J.M., Soto, J.I., Balanyá, J.C., 2002. Orthogonal folding of extensional detachments: Structure
817   and origin of the Sierra Nevada elongated dome (Betics, SE Spain). Tectonics 21, 3-1-3–20.
818   https://doi.org/10.1029/2001tc001283
819 Martínez-Martos, M., Galindo-Zaldivar, J., Martínez-Moreno, F.J., Calvo-Rayo, R., Galdeano, C.S. de, 2017.
820   Superposition of tectonic structures leading elongated intramontane basin: the Alhabia basin (Internal Zones,
821   Betic Cordillera). Int J Earth Sci 106, 2461–2471. https://doi.org/10.1007/s00531-016-1442-9
822 Meighan, H.E., Brink, U. ten, Pulliam, J., 2013. Slab tears and intermediate-depth seismicity: slab tears and
823   intermediate seismicity. Geophys Res Lett 40, 4244–4248. https://doi.org/10.1002/grl.50830
824 Meijninger, B.M.L., Vissers, R.L.M., 2006. Miocene extensional basin development in the Betic Cordillera, SE
825   Spain revealed through analysis of the Alhama de Murcia and Crevillente Faults: Miocene extensional basin
826   development in the Betic Cordillera. Basin Res 18, 547–571. https://doi.org/10.1111/j.1365-2117.2006.00308.x
827 Montenat, C., D'Estevou, P.O., 1992. Geodynamics of the Eastern Betic late Neogene Basins. A Review. Física de
828   la Tierra 57–75.
829 Mora, M., 1993. Tectonic and sedimentary analysis of the Huercal-Overa region, South East Spain, Betic Cordillera.
830   University of Oxford, 300 pp.
831 Mouthereau, F., Angrand, P., Jourdon, A., Ternois, S., Fillon, C., Calassou, S., Chevrot, S., Ford, M., Jolivet, L.,
832   Manatschal, G., Masini, E., Thinon, I., Vidal, O., Baudin, T., 2021. Cenozoic mountain building and topographic
833   evolution in Western Europe: impact of billions of years of lithosphere evolution and plate kinematics. Bsgf -
834   Earth Sci Bulletin 192, 56. https://doi.org/10.1051/bsgf/2021040

835 Mouthereau, F., Filleaudeau, P., Vacherat, A., Pik, R., Lacombe, O., Fellin, M.G., Castelltort, S., Christophoul, F.,
836   Masini, E., 2014. Placing limits to shortening evolution in the Pyrenees: Role of margin architecture and
837   implications for the Iberia/Europe convergence. Tectonics 33, 2283–2314. https://doi.org/10.1002/2014tc003663
838 Neuharth, D., Brune, S., Glerum, A., Morley, C.K., Yuan, X., Braun, J., 2021. Flexural strike-slip basins. Geology.
839   https://doi.org/10.1130/g49351.1
840 Nocquet, J.-M., 2012. Present-day kinematics of the Mediterranean: A comprehensive overview of GPS results.
841   Tectonophysics 579, 220–242. https://doi.org/10.1016/j.tecto.2012.03.037
842 Okay, A.I., Tüysüz, O., Kaya, Ş., 2004. From transpression to transtension: changes in morphology and structure
843   around a bend on the North Anatolian Fault in the Marmara region. Tectonophysics 391, 259–282.
844   https://doi.org/10.1016/j.tecto.2004.07.016
845 Palano, M., González, P.J., Fernández, J., 2015. The Diffuse Plate boundary of Nubia and Iberia in the Western
846   Mediterranean: Crustal deformation evidence for viscous coupling and fragmented lithosphere. Earth and
847   Planetary Science Letters 430, 439–447. https://doi.org/10.1016/j.epsl.2015.08.040
848 Palano, M., González, P.J., Fernández, J., 2013. Strain and stress fields along the Gibraltar Orogenic Arc:
849   Constraints on active geodynamics. Gondwana Res 23, 1071–1088. https://doi.org/10.1016/j.gr.2012.05.021
850 Palomeras, I., Thurner, S., Levander, A., Liu, K., Villaseñor, A., Carbonell, R., Harnafi, M., 2014. Finite-frequency
851   Rayleigh wave tomography of the western Mediterranean: Mapping its lithospheric structure. Geochemistry,
852   Geophysics, Geosystems 15, 140–160. https://doi.org/10.1002/2013gc004861
853 Pedrera, A., Galindo-Zaldívar, J., Galdeano, C.S. de, López-Garrido, Á.C., 2007. Fold and fault interactions during
854   the development of an elongated narrow basin: The Almanzora Neogene-Quaternary Corridor (SE Betic
855   Cordillera, Spain): FOLD AND FAULT INTERACTIONS. Tectonics 26, n/a-n/a.
856   https://doi.org/10.1029/2007tc002138
857 Pedrera, A., Galindo-Zaldívar, J., Ruíz-Constán, A., Duque, C., Marín-Lechado, C., Serrano, I., 2009. Recent large
858   fold nucleation in the upper crust: Insight from gravity, magnetic, magnetotelluric and seismicity data (Sierra de
859   Los Filabres–Sierra de Las Estancias, Internal Zones, Betic Cordillera). Tectonophysics 463, 145–160.
860   https://doi.org/10.1016/j.tecto.2008.09.037
861 Pedrera, A., Galindo-Zaldívar, J., Tello, A., Marín-Lechado, C., 2010. Intramontane basin development related to
862   contractional and extensional structure interaction at the termination of a major sinistral fault: The Huércal-
863   Overa Basin (Eastern Betic Cordillera). J Geodyn 49, 271–286. https://doi.org/10.1016/j.jog.2010.01.008
864 Peña, L.G. de la, Grevemeyer, I., Kopp, H., Díaz, J., Gallart, J., Booth-Rea, G., Gràcia, E., Ranero, C.R., 2020a. The
865   Lithospheric Structure of the Gibraltar Arc System From Wide-Angle Seismic Data. J Geophys Res Solid Earth
866   125. https://doi.org/10.1029/2020jb019854
867 Peña, L.G. de la, Ranero, C.R., Gràcia, E., 2018. The Crustal Domains of the Alboran Basin (Western
868   Mediterranean). Tectonics 37, 3352–3377. https://doi.org/10.1029/2017tc004946
869 Peña, L.G. de la, Ranero, C.R., Gràcia, E., Booth-Rea, G., 2020b. The evolution of the westernmost Mediterranean
870   basins. Earth-sci Rev 103445. https://doi.org/10.1016/j.earscirev.2020.103445
871 Pickering, K.T., Hodgson, D.M., Platzman, E., Clark, J.D., Stephens, C., 2001. A New Type of Bedform Produced
872   by Backfilling Processes in a Submarine Channel, Late Miocene, Tabernas-Sorbas Basin, SE Spain. J Sediment
873   Res 71, 692–704. https://doi.org/10.1306/2dc40960-0e47-11d7-8643000102c1865d
874 Pindell, J.L., Kennan, L., 2009. Tectonic evolution of the Gulf of Mexico, Caribbean and northern South America in
875   the mantle reference frame: an update. Geological Soc Lond Special Publ 328, 1–55.
876   https://doi.org/10.1144/sp328.1
877 Platt, J.P., Behr, W.M., Johanesen, K., Williams, J.R., 2013. The Betic-Rif Arc and Its Orogenic Hinterland: A
878   Review. Annual Review of Earth and Planetary Sciences 41, 313–357. https://doi.org/10.1146/annurev-earth-
879   050212-123951
880 Platt, J.P., Kelley, S.P., Carter, A., Orozco, M., 2005. Timing of tectonic events in the Alpujárride Complex, Betic
881   Cordillera, southern Spain. J Geol Soc London 162, 451–462. https://doi.org/10.1144/0016-764903-039
882 Platt, J.P., Vissers, R.L.M., 1989. Extensional collapse of thickened continental lithosphere: A working hypothesis
883   for the Alboran Sea and Gibraltar arc. Geology 17, 540–543. https://doi.org/10.1130/0091-
884   7613(1989)017<0540:ecotcl>2.3.co;2
885 Platt, J.P., Whitehouse, M.J., 1999. Early Miocene high-temperature metamorphism and rapid exhumation in the
886   Betic Cordillera (Spain): evidence from U–Pb zircon ages. Earth and Planetary Science Letters 171, 591–605.
887 Platzman, E.S., 1992. Paleomagnetic rotations and the kinematics of the Gibraltar arc. Geology 20, 311–314.
888   https://doi.org/10.1130/0091-7613(1992)020<0311:pratko>2.3.co;2

889 Poisson, A., Guezou, J.C., Ozturk, A., Inan, S., Temiz, H., Gürsöy, H., Kavak, K.S., ÖZDEN, S., 1996. Tectonic
890   Setting and Evolution of the Sivas Basin, Central Anatolia, Turkey. International Geology Review 38, 838–853.
891   https://doi.org/10.1080/00206819709465366
892 Poisson, A.M., Morel, J.L., Andrieux, J., Coulon, M., Wernli, R., Guernet, C., 1999. THE ORIGIN AND
893   DEVELOPMENT OF NEOGENE BASINS IN THE SE BETIC CORDILLERA (SE SPAIN): A CASE STUDY
894   OF THE TABERNAS-SORBAS AND HUERCAL OVERA BASINS. J Petrol Geol 22, 97–114.
895   https://doi.org/10.1111/j.1747-5457.1999.tb00461.x
896 Pourhiet, L.L., Huet, B., May, D.A., Labrousse, L., Jolivet, L., 2012. Kinematic interpretation of the 3D shapes of
897   metamorphic core complexes: 3D SHAPES OF MCCs. Geochem Geophys Geosystems 13.
898   https://doi.org/10.1029/2012gc004271
899 Pownall, J.M., Hall, R., Watkinson, I.M., 2013. Extreme extension across Seram and Ambon, eastern Indonesia:
900   evidence for Banda slab rollback. Solid Earth 4, 277–314. https://doi.org/10.5194/se-4-277-2013
901 Rat, J., Mouthereau, F., Brichau, S., Crémades, A., Bernet, M., Balvay, M., Ganne, J., Lahfid, A., Gautheron, C.,
902   2019. Tectonothermal Evolution of the Cameros Basin: Implications for Tectonics of North Iberia. Tectonics 38,
903   440–469. https://doi.org/10.1029/2018tc005294
904 Rat, J., Mouthereau, F., Brichau, S., Vacherat, A., Fillon, C., Gautheron, C., 2022. Timing and distribution of
905   exhumation in the Ebro basin reveal a plate-scale 10 Ma geodynamic event. Global Planet Change 103973.
906   https://doi.org/10.1016/j.gloplacha.2022.103973
907 Reicherter, K., Hübscher, C., 2006. Evidence for a seafloor rupture of the Carboneras Fault Zone (southern Spain):
908   Relation to the 1522 Almería earthquake? J Seismol 11, 15–26. https://doi.org/10.1007/s10950-006-9024-0
909 Reinhardt, L.J., Dempster, T.J., Shroder, J.F., Persano, C., 2007. Tectonic denudation and topographic development
910   in the Spanish Sierra Nevada. Tectonics 26, n/a-n/a. https://doi.org/10.1029/2006tc001954
911 Riding, R., Braga, J.C., Martín, J.M., Sánchez-Almazo, I.M., 1998. Mediterranean Messinian Salinity Crisis:
912   constraints from a coeval marginal basin, Sorbas, southeastern Spain. Mar Geol 146, 1–20.
913   https://doi.org/10.1016/s0025-3227(97)00136-9
914 Romagny, A., Jolivet, L., Menant, A., Bessière, E., Maillard, A., Canva, A., Gorini, C., Augier, R., 2020. Detailed
915   tectonic reconstructions of the Western Mediterranean region for the last 35 Ma, insights on driving
916   mechanisms. Bsgf - Earth Sci Bulletin 191, 37. https://doi.org/10.1051/bsgf/2020040
917 Rosenbaum, G., Lister, G.S., Duboz, C., 2002. Relative motions of Africa, Iberia and Europe during Alpine
918   orogeny. Tectonophysics 359, 117–129. https://doi.org/10.1016/s0040-1951(02)00442-0
919 Sanz de Galdeano, C.S., Vera, J.A., 1992. Stratigraphic record and palaeogeographical context of the Neogene
920   basins in the Betic Cordillera, Spain. Basin Res 4, 21–36. https://doi.org/10.1111/j.1365-2117.1992.tb00040.x
921 Sanz de Galdeano, C.S.D., Rodriguez-Fernandez, J., Lopez-Garrido, A.C., 1985. A strike-slip fault corridor within
922   the Alpujarra Mountains (Betic Cordilleras, Spain). Geol Rundsch 74, 641–655.
923   https://doi.org/10.1007/bf01821218
924 Sanz de Galdeano, C.S. de, Alfaro, P., 2004. Tectonic significance of the present relief of the Betic Cordillera.
925   Geomorphology 63, 175–190. https://doi.org/10.1016/j.geomorph.2004.04.002
926 Scotney, P., Burgess, R., Rutter, E.H., 2000. 40Ar/39Ar age of the Cabo de Gata volcanic series and displacements
927   on the Carboneras fault zone, SE Spain. J Geol Soc London 157, 1003–1008.
928   https://doi.org/10.1144/jgs.157.5.1003
929 Sosson, M., Morrillon, A.-C., Bourgois, J., Féraud, G., Poupeau, G., Saint-Marc, P., 1998. Late exhumation stages
930   of the Alpujarride Complex (western Betic Cordilleras, Spain): new thermochronological and structural data on
931   Los Reales and Ojen nappes. Tectonophysics 285, 253–273. https://doi.org/10.1016/s0040-1951(97)00274-6
932 Spakman, W., Wortel, R., 2004. The TRANSMED Atlas. The Mediterranean Region from Crust to Mantle 31–52.
933   https://doi.org/10.1007/978-3-642-18919-7_2
934 Stich, D., Serpelloni, E., Mancilla, F. de L., Morales, J., 2006. Kinematics of the Iberia–Maghreb plate contact from
935   seismic moment tensors and GPS observations. Tectonophysics 426, 295–317.
936   https://doi.org/10.1016/j.tecto.2006.08.004
937 Teyssier, C., Tikoff, B., 1998. Strike-slip partitioned transpression of the San Andreas fault system: a lithospheric-
938   scale approach. Geological Soc Lond Special Publ 135, 143–158. https://doi.org/10.1144/gsl.sp.1998.135.01.10
939 Vacherat, A., Mouthereau, F., Pik, R., Bellahsen, N., Gautheron, C., Bernet, M., Daudet, M., Balansa, J., Tibari, B.,
940   Jamme, R.P., Radal, J., 2016. Rift-to-collision transition recorded by tectonothermal evolution of the northern
941   Pyrenees. Tectonics 35, 907–933. https://doi.org/10.1002/2015tc004016
942 Vázquez, M., Jabaloy, A., Barbero, L., Stuart, F.M., 2011. Deciphering tectonic- and erosion-driven exhumation of
943   the Nevado-Filábride Complex (Betic Cordillera, Southern Spain) by low temperature thermochronology:

944   Deciphering tectonic- and erosion-driven exhumation. Terra Nova 23, 257–263. https://doi.org/10.1111/j.1365-
945   3121.2011.01007.x
946 Vergés, J., Fernàndez, M., 2012. Tethys–Atlantic interaction along the Iberia–Africa plate boundary: The Betic–Rif
947   orogenic system. Tectonophysics 579, 144–172. https://doi.org/10.1016/j.tecto.2012.08.032
948 Vernant, P., Fadil, A., Mourabit, T., Ouazar, D., Koulali, A., Davila, J.M., Garate, J., McClusky, S., Reilinger, R.,
949   2010. Geodetic constraints on active tectonics of the Western Mediterranean: Implications for the kinematics and
950   dynamics of the Nubia-Eurasia plate boundary zone. J Geodyn 49, 123–129.
951   https://doi.org/10.1016/j.jog.2009.10.007
952 Villasenor, A., Chevrot, S., Harnafi, M., Gallart, J., Pazos, A., Serrano, I., Córdoba, D., Pulgar, J.A., Ibarra, P.,
953   2015. Subduction and volcanism in the Iberia–North Africa collision zone from tomographic images of the
954   upper mantle. Tectonophysics. https://doi.org/10.1016/j.tecto.2015.08.042
955 Waldner, M., Bellahsen, N., Mouthereau, F., Bernet, M., Pik, R., Rosenberg, C.L., Balvay, M., 2021. Central
956   Pyrenees Mountain Building: Constraints From New LT Thermochronological Data From the Axial Zone.
957   Tectonics 40. https://doi.org/10.1029/2020tc006614
958 Weijermars, R., Roep, Th.B., Eeckhout, B.V. den, Postma, G., Kleverlaan, K., 1985. Uplift history of a Betic fold
959   nappe inferred from Neogene-Quaternary sedimentation and tectonics (in the Sierra Alhamilla and Almeria,
960   Sorbas and Tabernas Basins of the Betic Cordilleras, SE Spain). Geologie en Mijnbouw 397–411.
961 Zeck, H.P., Monié, P., Villa, I.M., Hansen, B.T., 1992. Very high rates of cooling and uplift in the Alpine belt of the
962   Betic Cordilleras, southern Spain. Geology 20, 79. https://doi.org/10.1130/0091-
963   7613(1992)020<0079:vhroca>2.3.co;2
964